Published in the Annual Review of
Nuclear Science, Vol. 27, 393 - 464
(1977)

PSIONIC MATTER

W. Chinowsky

December 1977

Prepared for the U. S. Department of Energy
under Contract W-7405-ENG-48

DISCLAIMER

Ann. Rev. Nucl. Sci. 1977. 27: 393–464

PSIONIC MATTER[1]

*5589

W. Chinowsky
Department of Physics and Lawrence Berkeley Laboratory, University of California, Berkeley, California 94720

CONTENTS

[1] Work supported by the Energy Research and Development Administration, under the auspices of the Division of Physical Research.

INTRODUCTION

Before November of 1974, heavy hadrons that decay to hadrons were neatly classified into two groups, distinguished by their decay rates. Those are, very roughly, either of the order of 10^{-9} sec or 10^{-23} sec (1). Strangeness conservation distinguishes the longer-lived group from the shorter-lived one. The strikingly different decay rate of the J/ψ,[2] orders of magnitude different from either of these values, indicates the operation of a quite different kind of dynamics. With further developments, particularly the observation in e^+e^- annihilation of heavier, directly formed vector states as well as others produced in e^+e^- annihilations to multiparticle states, interpretation has narrowed. Arguments in favor of a new property of matter and a new conservation law for strong interactions have become very convincing, if not yet entirely compelling. Indeed, all observations now fit very comfortably into a theoretical framework originating with the introduction of a fourth quark precisely of the character proposed earlier, and for quite different reasons, by Glashow and co-workers (2, 3). In this article, I review the phenomenology of psion production and decay, and also charmed-hadron production and decay, as relevant to a broader conception of the subject. The simple model of the ψ states as composites of a charmed quark and its antiparticle dominates the interpretive discussion (4, 5).

1.1 *Old Vector Mesons*

It is inappropriate to give an extensive review of properties of the older hadronic resonant states, but still useful to summarize some characteristics of production and decay to contrast with the ψ-family characteristics. Only those vector mesons that couple directly to the photon, i.e. ρ^0, ω^0, and ϕ^0, are discussed. Table 1 shows selected decay parameters of these vector mesons (1). Values of full width, Γ, and partial width, Γ_{ee}, for decay to e^+e^- pairs, have been extracted from measurements of cross sections for e^+e^- annihilation to particular hadronic final states, $\pi^+\pi^-$ for ρ^0, $\pi^+\pi^-\pi^0$ for ω^0, and $K\bar{K}$ for ϕ (6). The annihilation cross section in the vicinity of a resonance varies with center of mass (c.m.) energy E, according to the Breit-Wigner expression

$$\sigma_f(E) = \frac{(2J+1)\pi}{E^2} \frac{\Gamma_{ee}\Gamma_f}{(E-M)^2+\Gamma^2/4},$$

Table 1 Parameters of vector mesons ρ^0, ω^0, and ϕ^0

Meson	Mass (MeV/c^2)	Γ(MeV)	Γ_{ee}(keV)	$f_v^2/4\pi$
ρ^0	773 ± 3	152 ± 3	6.5 ± 0.7	2.1 ± 0.2
ω^0	782.7 ± 0.3	10.0 ± 0.4	0.76 ± 0.17	18.3 ± 4.0
ϕ^0	1019.7 ± 0.3	4.1 ± 0.2	1.31 ± 0.08	13.8 ± 0.8

[2] From now on, I eschew the typographically awkward "J/ψ" and use ψ or ψ (3095) for the lightest psion.

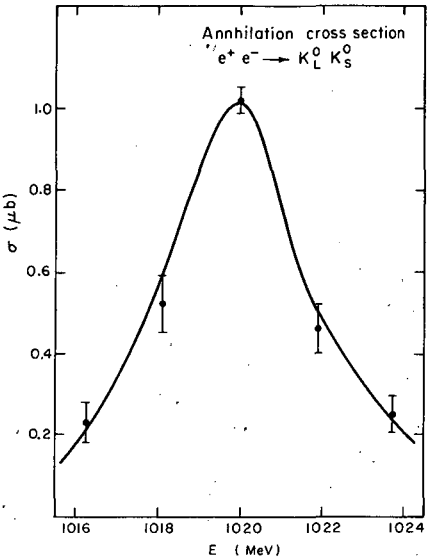

Figure 1 Cross section for e^+e^- annihilation to $K_S^0K_L^0$ as a function of c.m. energy, showing ϕ^0-meson resonance excitation; data from (7).

where Γ_f and Γ_{ee} are the partial widths for decay to the final states f and e^+e^- respectively, and Γ is the full width. Suitable modification of this simple behavior must be made to take account of initial-state radiation in order to obtain the resonance widths. An exemplary excitation curve, for $K_L^0K_S^0$ production (7), is shown in Figure 1. The full width and the product $\Gamma_{ee}\Gamma_f$ are determined from the annihilation cross sections near the resonance. Values of Γ_f are obtained from independent sources, thus allowing determination of electron-pair partial widths. A useful parameterization is in terms of the coupling of the vector meson to the virtual photon, indicated in the vector-dominance (8) diagram of Figure 2. The coupling constant f_v, defined by

$$G_v \equiv M_v^2/f_v,$$

is related to Γ_{ee} by (9)

$$f_v^2/4\pi = \frac{1}{3}\frac{\alpha^2 M_v}{\Gamma_{ee}}. \qquad 1.1$$

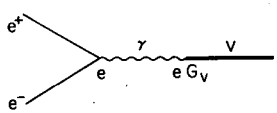

Figure 2 Direct coupling of a vector meson to a virtual photon.

Values of Γ in Table 1 are averages of values obtained from measurements of resonance production in hadron-hadron interactions, as well as the e^+e^- annihilation results. As has been remarked often, it is noteworthy that the width of the ϕ^0 is only one half that of the ω^0 and more remarkable still that the partial width for ϕ^0 decay to $\pi^+\pi^-\pi^0$ is just 0.67 ± 0.07 MeV, while the partial width is 9.0 ± 0.4 MeV for decay of the lighter ω^0 to $\pi^+\pi^-\pi^0$. Indeed the principal decay mode of the ϕ^0 meson is $K\bar{K}$, with 82% branching fraction, in spite of the relatively small phase space that is available to that state.

Meson resonances of the old style are produced in hadron-hadron collisions, restricted only by requirements of the strong-interaction conservation laws. Typical exclusive reaction cross sections, e.g. for $\pi p \to \rho p$, are in the range 0.1–10 mb (10), values typical of strong interactions. Data on inclusive vector-meson production in hadron-hadron interactions are sparse and suffer poor statistical accuracy. Inclusive ρ^0 production rates in π-p and p-p collisions have been determined from observations of interactions in bubble chambers (11). Cross sections increase smoothly from ~ 2 mb at 4.9 GeV c.m. energy to ~ 10 mb at 19 GeV. Inclusive production of ϕ^0 appears to be smaller by about a factor of ten, judging from measured values of 0.16 ± 0.04 mb at 6.8 GeV (12) and 0.6 ± 0.2 mb at 16.8 GeV c.m. energy (13). The first result is again from a pp bubble-chamber exposure. The other is from an experiment that measured rates for muon pair production in π^+ and proton collisions with Be nuclei. It is described in some detail below.

In the context of vector-meson dominance (8), vector-meson photoproduction (14) and scattering are related according to (15)

$$\frac{d\sigma}{dt}(\gamma p \to Vp) = \frac{4\pi}{f_v^2} \alpha \frac{d\sigma}{dt}(Vp \to Vp) \qquad 1.2$$

where t is the momentum transfer. With the optical theorem, neglecting the real part of the forward scattering amplitude,

$$\frac{d\sigma}{dt}(\gamma p \to Vp) = \frac{\alpha}{16\pi} \frac{4\pi}{f_v^2} \sigma_T^2(Vp \to Vp) \qquad 1.3$$

at $t = 0$. The value of the total vector-meson-nucleon interaction cross section, σ_T, is then obtained with f_v determined from the e^+e^- partial width Γ_{ee}.

Values of $d\sigma/dt$ at $t = 0$ for ρ^0 photoproduction on protons are, to within $\sim 15\%$, constant at 115 μb/GeV^2 for 3.6 GeV $< (s)^{1/2} <$ 5.9 GeV (16). Using the vector-

Table 2 Properties of quarks

Flavor	Spin	I	I_3	Q/e	B	S	Y	C
u	1/2	1/2	1/2	2/3	1/3	0	1/3	0
d	1/2	1/2	−1/2	−1/3	1/3	0	1/3	0
s	1/2	0	0	−1/3	1/3	−1	−2/3	0
c	1/2	0	0	2/3	1/3	0	0	1

dominance equation (1.3) with $f_\rho^2/4\pi$ determined from a weighted average of measured $e^\pm$ and $\mu^\pm$ partial widths (1), we obtain the total cross section $\sigma(\rho\text{-nucleon}) = 24$ mb in that range of c.m. energy. Results of measurements of ϕ^0 photoproduction (17) at various energies in the range 2.2 GeV $< (s)^{1/2} <$ 4.2 GeV are compatible with a constant value for the differential cross section at $t = 0$, $d\sigma/dt = 2.49 \pm 0.15$ μb GeV^{-2}. Vector dominance then yields $\sigma(\phi\text{-nucleon}) = 8.7 \pm 0.5$ mb (17). Those values for ρ^0 and for ϕ^0 interaction cross sections are typical of strong interactions.

1.2 *Quark-Model Classification*

Hadron states group into multiplets specified by spin, parity, and baryon numbers indicative of the exact SU(2) symmetry and approximate SU(3) symmetry of the strong interactions. Baryons populate SU(3) multiplets of dimensionality ten and eight. Mesons fit into octet and singlet representations. The observed states can be considered composite structures whose basic constituents are the three spin-$\frac{1}{2}$ quarks of the 3 representation of SU(3). Their properties are listed in Table 2. In this model, baryons are systems of three quarks, and mesons are quark-antiquark composites. Properties of meson states are given in terms of the orbital and spin angular momentum of the $q\bar{q}$ system and its isospin, namely spin $J = |\mathbf{L}+\mathbf{S}|$, parity $P = (-1)^{L+1}$, charge conjugation $C = (-1)^{L+S}$ and G-parity $G = C(-1)^I$. Members of the lowest-lying meson multiplets are s states of the $q\bar{q}$ system. The quark contents assigned to the "old" vector mesons are

$$\rho^0 = (2)^{-1/2}[u\bar{u} - d\bar{d}]$$

$$\omega^0 = (2)^{-1/2}[u\bar{u} + d\bar{d}]$$

$$\phi^0 = s\bar{s}.$$

An essentially ad hoc rule based on this composition and those of the pseudoscalar mesons, the Okubo (18)-Zweig (19)-Iizuka (20) (OZI) rule, has been introduced to explain the small width and dominant $K\bar{K}$ decay mode of the ϕ. This rule proclaims that a process is inhibited if its duality diagram contains disconnected quark lines. Such lines can be isolated in a duality diagram by drawing a line that crosses no quark lines. Allowed and forbidden decays of the ϕ-meson are illustrated in Figure 3. Some attempts have been made to put the OZI rule on a firmer dynamical foundation based on dual models (21) or asymptotically free gauge theories (22), but only semiquantitative success has yet been achieved.

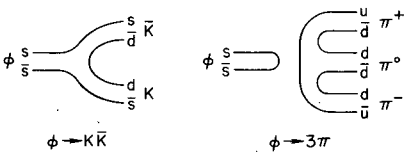

Figure 3 Duality (quark-line) diagrams for $K\bar{K}$, OZI-allowed; and 3π, OZI-forbidden, decays of the ϕ meson.

2 PRODUCTION OF $\psi(3095)$ AND $\psi(3684)$

The existence of the narrow state $\psi(3095)$ was first established independently, with quite different experimental techniques, by Aubert et al (23) and Augustin et al (24).

The Brookhaven National Laboratory-Massachussets Institute of Technology (BNL-MIT) (23) group measured the effective mass spectrum of e^+e^- pairs produced in the interaction of 28.5 GeV/c protons with beryllium, $p + \text{Be} \rightarrow e^+ + e^- + X$. In this experiment, a double-arm magnetic spectrometer, designed to have maximum detection efficiency for heavy, unstable particles produced at rest in the center of mass, produced the mass spectrum shown in Figure 4. A narrow resonance was definitively established at mass 3.112 GeV/c^2 and width less than the 5-MeV/c^2 experimental resolution of the apparatus. More details of this experiment and subsequent hadronic-production experiments are given below.

The Lawrence Berkeley Laboratory-Stanford Linear Accelerator Center (LBL-SLAC) (24) group measured the total cross section for e^+e^- annihilation as a function of energy. Measurements were made in small energy intervals near 3100 MeV with a

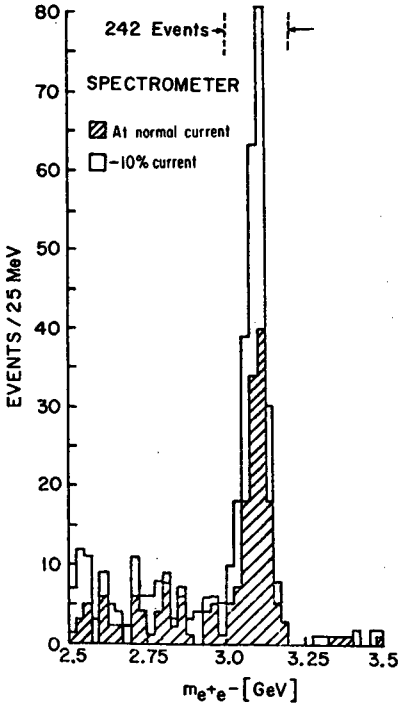

Figure 4 Invariant-mass spectrum of e^+e^- pairs produced in collisions of 28-GeV/c protons with beryllium showing J-meson production; from (23).

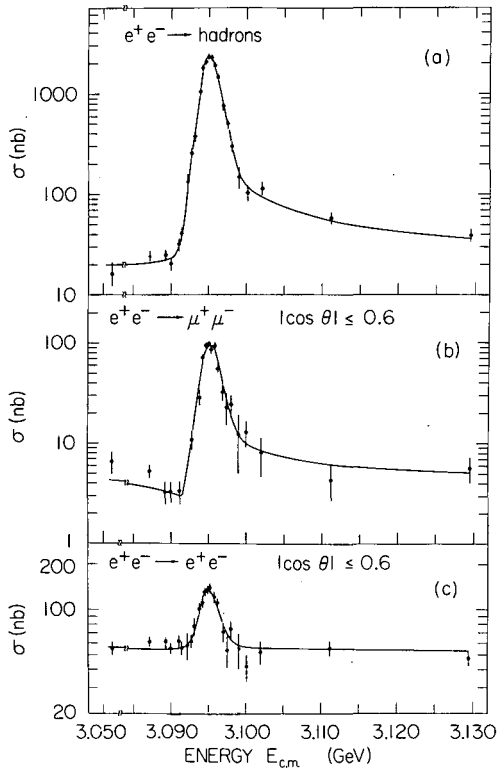

Figure 5 Cross sections for e^+e^- annihilation to (*a*) hadrons, (*b*) muon pairs, and (*c*) electron pairs, showing ψ(3095)-resonance excitation; from (43).

cylindrical detector array in an axially directed solenoidal magnetic field. Yields were measured for annihilation to e^+e^- pairs, $\mu^+\mu^-$ pairs, and multiparticle hadronic states. Results, shown in Figure 5, indicate a resonance at 3095 MeV, coupled to e^+e^-, $\mu^+\mu^-$, and hadronic states. Its width is less than 2 MeV. With the same technique, the LBL-SLAC group observed a second resonance at 3684 MeV, as indicated by the data of Figure 6 (25). Again the hadronic and lepton-pair decay modes appear, with the latter less prominent than at 3095 MeV.

The ψ resonance peak has been observed in e^+e^- annihilations at the storage ring ADONE (26); both ψ and ψ' have been observed at the higher-energy e^+e^- storage rings DORIS (27). Those results confirmed the existence of the two states and generally agree with the SLAC-LBL measurements of energy and decay widths of the resonances.

Further analyses of the shapes of these yield curves, particularly by the LBL-SLAC group, taking account of broadening due to finite beam-energy spread and initial-state radiation, led to determination of the full widths 69 ± 15 keV and

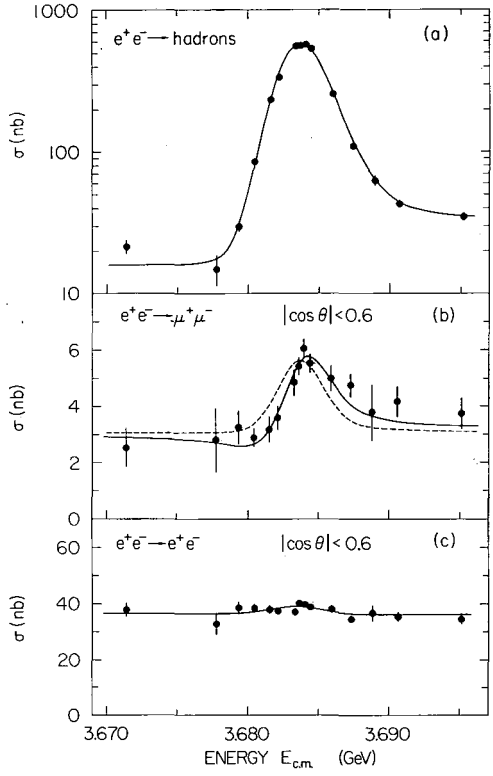

Figure 6 Cross sections for e^+e^- annihilation to (*a*) hadrons, (*b*) muon pairs, and (*c*) electron pairs, showing $\psi(3684)$ resonance excitation; from (51).

228 ± 56 keV for the lower- and higher-mass resonances, respectively. Compared with previously established resonances at considerably smaller energies, these widths are startingly small, indicating the effect of some new mechanism inhibiting their decays.

2.1 *Production of ψ and ψ' in Hadron-Hadron Collisions*

All such experiments have until now searched for narrow peaks in mass distributions of pairs of oppositely charged leptons as a signature of decays of heavy particles produced in the primary hadronic reactions. Severe experimental difficulties in detecting decay products in heavy backgrounds of hadronic debris have been overcome with sophisticated, complex experimental arrangements with special capabilities (28, 29). These include $e^\pm$ or $\mu^\pm$ identification and rejection of $\pi^\pm$, $K^\pm$, $p^\pm$; momentum- and angle-measurement precision sufficient to yield mass resolution of order 10–100 MeV/c^2; multicoincident counting of particles to reduce accidental rates to acceptable levels; good multitrack efficiency and position resolution; rejection of photon and neutron backgrounds associated with incident beams and

from secondary, diffuse sources; large angle and large mass acceptance; and, since rates are very low, reliability over long periods of experimental operation. Instrumental limitations restrict the detected regions of production and decay phase space, and further introduce mass dependence in the acceptance of the apparatus. To obtain absolute yields, corrections must be made for these geometric deficiencies, as well as detection inefficiencies. Calculations are made with Monte Carlo simulations of detector response with an assumed dependence on production and decay kinematic variables.

2.1.1 28.5-GeV/c AND 20-GeV/c PROTONS ON BERYLLIUM Aubert et al (BNL-MIT) (30) used an arrangement designed for maximum acceptance of heavy particles produced at rest in the center of mass in the reaction $p+\mathrm{Be} \rightarrow e^+e^- + X$ (X signifies all other particles in the final state). The experiment was made with incident protons of 28.5 GeV/c momentum. Schematic views of the detector are shown in Figure 7. To extract a ψ production cross section from the observed peak in the mass distribution, they assumed the differential cross section

$$\frac{\mathrm{d}^3\sigma}{\mathrm{d}P_{\parallel}^{*}\,\mathrm{d}P_{\perp}^{*2}} \propto \frac{\exp(-6P_{\perp}^{*})}{E^{*}}$$

for production of a ψ with c.m. longitudinal momentum $P_{\parallel}^{*}$ and transverse momentum $P_{\perp}^{*}$ and allowed the ψ decay to be isotropic at rest. They obtained a

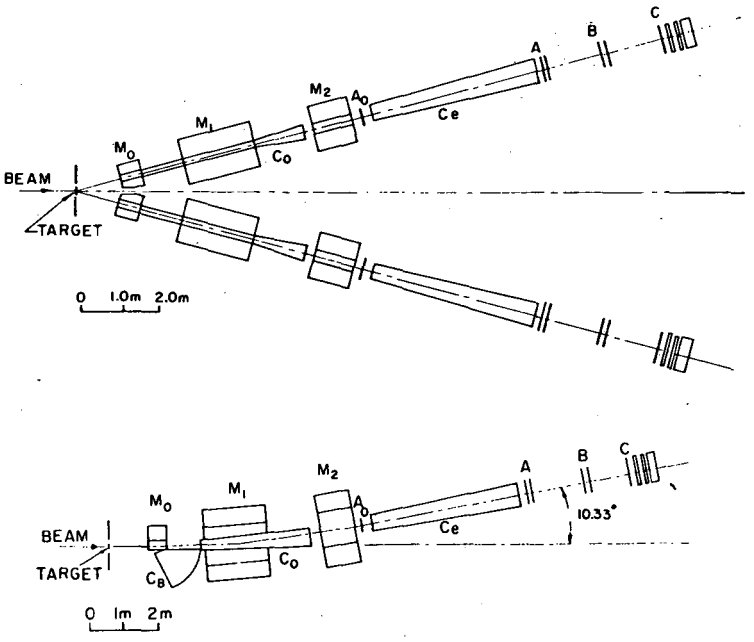

Figure 7 Spectrometer detection apparatus of the MIT-BNL group (23, 28–30) at Brookhaven National Laboratory.

production cross section $\sigma \sim 10^{-34}$ cm^2/nucleon for e^+e^- pairs with mass in the peak. With 20-GeV/c incident protons, the cross section is ten times smaller. No production of heavier particles was observed, again at 28.5 GeV/c, yielding an estimated upper limit $\sigma \sim 10^{-36}$ cm^2, with 95% confidence, for e^+e^- pairs of mass 3.2 GeV/c^2 $< M <$ 4.0 GeV/c^2.

2.1.2 300-GeV NEUTRONS ON NUCLEI Knapp et al (31) and later, Binkley et al (32, 33), measured the yield of muon pairs in interactions of neutrons with Be, Al, Cu, and Pb nuclei. A primary objective was to determine the A dependence of resonance production so that cross sections for single nucleon interaction could be determined by extrapolation. Neutrons were produced by 300-GeV/c protons in the earlier experiments and by 400-GeV/c protons in the later runs. The resultant neutron-energy spectra peak at ~250 GeV and ~300 GeV for the lower and higher proton energy, respectively. Binkley et al (32) made fits to the yields of dileptons of momentum $p < 75$ GeV/c with the power law A^γ, obtaining the best-fit value $\gamma = 0.93 \pm 0.04$ for $\psi(3095)$ production. In contrast, they find $\gamma = 0.62 \pm 0.03$ for ρ^0 and ω^0. Fits were made to the observed distributions in the dimuons' $P_\perp$ and $P_\parallel$ (Figure 8), taking account of acceptance limitations and resolution, using assumed production dependences on x ($\equiv P^*_\parallel/P^*_{max}$) and $P_\perp$ of the form

$$E\frac{d^3\sigma}{dP^3} = C(1-x)^\alpha \exp(-bP_\perp) \qquad \text{for} \quad x_0 < x < 1,$$

and

$$E\frac{d^3\sigma}{dP^3} = C(1-x_0)^\alpha \exp(-bP_\perp) \qquad \text{for} \quad 0 < x < x_0.$$

For dimuon decay products of $\psi(3095)$, they obtain values $\alpha = 5.2 \pm 0.5$, $b = (1.6 \pm 0.2)$ c GeV^{-1} with $x_0 = 0.3$. With these, they calculated an integrated yield of ψ-

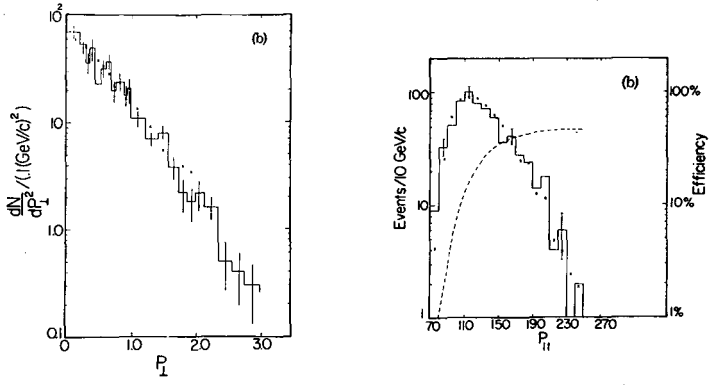

Figure 8 Differential yield of ψ mass dimuons as functions of transverse ($P_\perp$) and longitudinal ($P_\parallel$) momentum from interactions of ~300-GeV neutrons with nuclei; ×'s are results of a Monte Carlo calculation; from (33).

mass $\mu^{\pm}$ pairs

$$\int_{0.24}^{1.0} B_{\mu\mu} \frac{d\sigma}{dx} dx \simeq 3.5 \times 10^{-33} \text{ cm}^2/\text{nucleon}.$$

With the further assumption $d\sigma/dy = \text{constant}$ ($y \equiv$ c.m. rapidity) in the region $0 < x < 0.3$, extrapolation into the unobservable region $x < 0.24$ yields the estimate for product of branching ratio, $B_{\mu\mu}$, and total inclusive cross section, $B_{\mu\mu}\sigma = 22 \times 10^{-33}$ cm^2/nucleon for 300-GeV neutrons. With no evidence for ψ' production, they conclude

$$B_{\mu\mu}(\psi')\sigma(\psi')/B_{\mu\mu}(\psi)\sigma(\psi) < 0.015.$$

2.1.3 150-GeV/c π^+ AND PROTONS ON BERYLLIUM An extensive series of measurements of inclusive $\mu^{\pm}$ production by 150-GeV/c protons and positive pions on Be has been carried out by Anderson et al (34, 35). Muon pairs with mass 0.456 GeV/$c^2 < M <$ 3.5 GeV/c^2 were detected efficiently, so that ρ^0 (or ω^0) and ϕ^0 decays were observed, as well as ψ decays. Their apparatus is shown in Figure 9. Muons are specified by the requirement that they penetrate a total of 4.7-m iron absorber. The observed dependence of dimuon yield on x and transverse momentum $P_\perp$ of the dimuon was fit with a parameterization of the invariant differential cross section, also of the form

$$E\frac{d^3\sigma}{dP^3} = C(1-x)^{\alpha} \exp(-bP_\perp)$$

after appropriate corrections for detection efficiency. Events with $x > 0.15$ and $P_\perp > 200$ MeV/c were included in the fits. For the dependence of $\psi(3095)$ yield on x, they find $\alpha = 2.9 \pm 0.3$ for production by protons and $\alpha = 1.7 \pm 0.4$ for production by pions. The steeper x dependence with incident protons than with pions agrees with earlier results of Blanar et al (36) for π^- and proton interactions with iron. The parameters of the $P_\perp$ dependence obtained are $b = 2.1 \pm 0.3$ c GeV^{-1} and $b = 2.6 \pm 0.4$ c GeV^{-1} for incident protons and pions, respectively. It is worth noting that the falloff with $P_\perp$ is significantly slower than that observed for ρ^0 (or ω^0) or ϕ^0 production, for which the corresponding parameter $b \sim 4$ for protons or pions. Integrated inclusive cross sections for production on single nucleons,

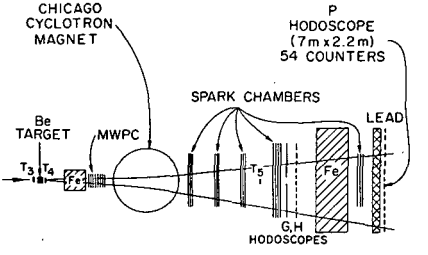

Figure 9 Spectrometer detection apparatus of Anderson et al (34) at Fermi National Accelerator Laboratory.

obtained by extrapolating the fit of $d\sigma/dx$ to $x = 0$ and using the dependence on A of (32), are $\sigma_p B_{\mu\mu} = (3.3 \pm 1.1) \times 10^{-33}$ cm^2/nucleon for incident protons and $\sigma_\pi B_{\mu\mu} = (6.5 \pm 2.2) \times 10^{-33}$ cm^2/nucleon for incident pions, for forward, $x > 0$, psions.

2.1.4 70-GeV/c PROTONS ON BERYLLIUM An arrangement similar to the above was used by Antipov et al (37) to measure $\mu^\pm$ pair yields from 70 GeV/c protons on beryllium. They fit the x distribution for ψ production with $\exp[-(6.0 \pm 1.2)x]$ for $x > 0.3$ and constant at smaller x. The $P_\perp$ dependence has the form

$$d\sigma/dP_\perp^2 \sim \exp[-(1.8 \pm 0.03)P_\perp^2].$$

For the inclusive $\psi(3095)$ production yield, they obtained

$$\sigma B_{\mu\mu} = (9.5 \pm 2.5) \times 10^{-33} \text{ cm}^2\text{/nucleus},$$

and, with the $A^{0.93}$ dependence of Binkley et al,

$$\sigma B_{\mu\mu} = (1.2 \pm 0.3) \times 10^{-33} \text{ cm}^2\text{/nucleon},$$

2.1.5 400-GeV PROTONS ON Be Hom et al (38, 40) and Snyder et al (39) have measured both $e^\pm$ and $\mu^\pm$ pair yields from interactions of 400-GeV protons with beryllium. Their spectrometer acceptance limits the detectable phase space to the small x interval $-0.06 < x < 0.08$ and to $P_\perp < 2$ GeV/c. They observed a transverse-momentum dependence well represented by either

$$E\frac{d^3\sigma}{dP^3} = (1.7 \pm 0.4) \times 10^{-32} \exp[-(1.1 \pm 0.4)P_\perp^2] \text{ cm}^2\text{/nucleus}$$

or

$$E\frac{d^3\sigma}{dP^3} = (2.5 \pm 0.6) \times 10^{-32} \exp[-(1.6 \pm 0.4)P_\perp] \text{ cm}^2\text{/nucleus}.$$

That result, extrapolated away from $x \simeq 0$ with the functional form

$$E\frac{d^3\sigma}{dP^3} = C(1-x)^{4.3} \exp(-1.6\,P_\perp),$$

yields an inclusive cross-section branching-ratio product

$$\sigma B = (1.0 \pm 0.3) \times 10^{-31} \text{ cm}^2\text{/nucleus},$$

which gives, with $A^{0.93}$ dependence,

$$\sigma B = (1.3 \pm 0.3) \times 10^{-32} \text{ cm}^2\text{/nucleon}.$$

A small peak at a mass consistent with ψ' yields an estimate of the ratio of production cross sections $\sigma(\psi')/\sigma(\psi) = (10 \pm 3)\%$.

2.1.6 26-GeV PROTONS ON 26-GeV PROTONS In p-p collisions at the CERN Intersecting Storage Rings (ISR), production of ψ has been observed, with ψ identified by e^+e^- (41) and $\mu^+\mu^-$ (42) decays. From the $\mu^+\mu^-$ yield at c.m. energy $(s)^{1/2} = 52$

GeV, there results an estimate of total cross section $\sigma B = (4.2 \pm 1.9) \times 10^{-32}$ cm^2, based on detection of eleven dimuon events above background.

2.1.7 SUMMARY Dividing the measured values of dilepton yields by $B_{\mu\mu} = 0.069$, the branching ratio for $\psi(3095)$ decay to lepton pairs obtained by the LBL-SLAC group (43), one obtains the various ψ-production total cross-section estimates plotted as a function of c.m. energy in Figure 10. This shows a rise of more than two orders of magnitude from the lowest energy, $(s)^{1/2} = 7.4$ GeV, to the highest, $(s)^{1/2} = 52$ GeV. Cross sections for ϕ production are smaller than those for ρ by about a factor of ten. Production of the ψ's is more grossly inhibited; their rates are a factor of 1000 smaller still. Average transverse momenta of the ψ's are about 1 GeV/c, roughly twice as large as those of ρ^0 and ϕ^0.

2.2 *Photoproduction of ψ and ψ'*

Measurement of the ψ differential photoproduction cross section, extrapolated to $t = 0$, with application of the vector-meson dominance-model prescription, yields

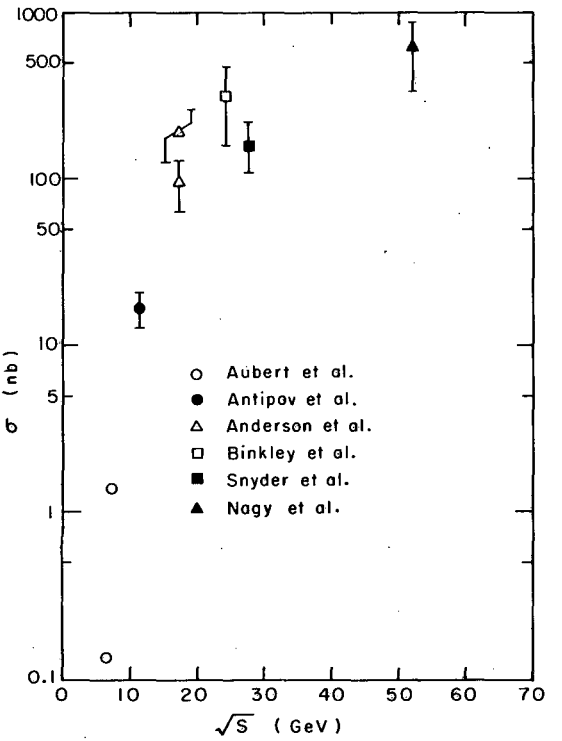

Figure 10 Compendium of results on the energy dependence of the cross section for inclusive $\psi(3095)$ production in hadron-hadron collisions; data from (30, 32–39, 42).

estimates of the ψ-nucleon total cross section (see Section 1.1) and so is important for determination of the strength of ψ coupling to hadrons.

Knapp et al (44) first observed ψ photoproduction and its diffractive character. Photons were produced by 300-GeV protons interacting with beryllium and had a continuous energy distribution to a maximum of ~200 GeV. The photon beam bombarded a beryllium target, and produced muon pairs were detected. Camerini et al (45) observed production of electron pairs and muon pairs, made by bremsstrahlung photons of various energies from 13 GeV to 21 GeV, interacting with deuterium. Gittelman et al (46) measured ψ production by 11.8-GeV bremsstrahlung photons on a beryllium target, detecting electron-pair decays. Nash et al (47) measured electron-pair yields from bombardment of deuterium by photons of mean energy 55 GeV, in a range from 31–80 GeV. A typical yield curve is in Figure 11, showing the electron-pair effective mass distribution produced in the experiment of Gittelman et al. Figure 12, the momentum-transfer distribution of dimuon pairs with mass near 3100 MeV/c^2, the results of Knapp et al, shows the characteristic

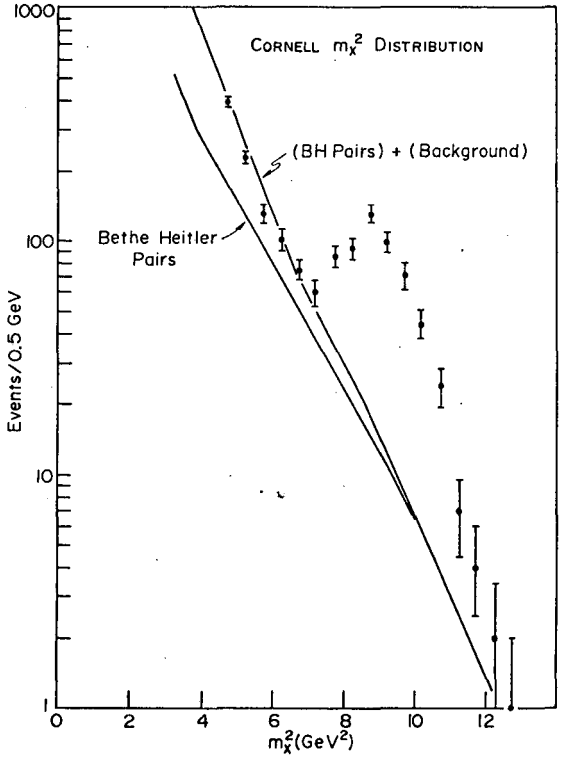

Figure 11 Invariant-mass distribution of dielectrons photoproduced on beryllium at 11 GeV, showing ψ(3095) yield; from (46).

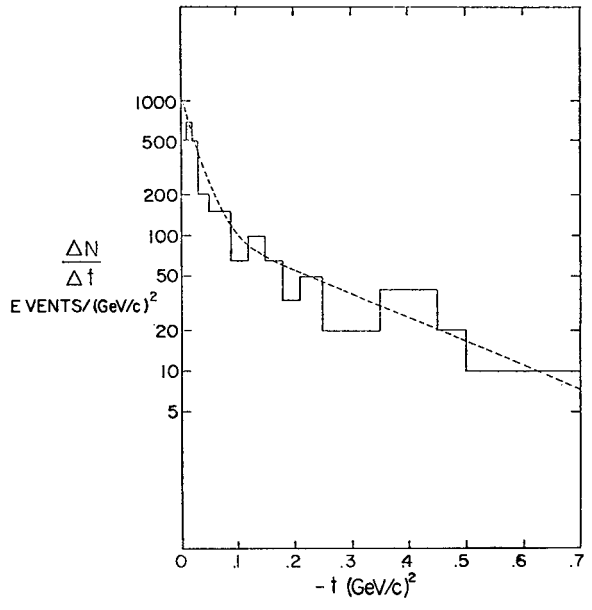

Figure 12 Differential yield of $\psi(3095)$ photoproduction on beryllium as a function of momentum transfer. The superimposed curve is the calculated t distribution of the form $A^2 \exp(40t) + A \exp(4t)$ after correction for experimental resolution and detector acceptance; from (44).

exponential behavior near zero momentum transfer. In a subsequent experiment at SLAC, Camerini et al (45) detected single-muon decay products of $\psi(3095)$ produced by photons on beryllium and tantalum. They provide a measurement of photoproduction rates for, among others, 9.5-GeV incident energy, the lowest energy at which $\psi(3095)$ photoproduction has been observed and find, in fact, the smallest differential cross section, 0.18 ± 0.08 nb $(\text{GeV}/c)^{-2}$ at the minimum momentum transfer. We have applied the vector-dominance relation (Equation 1.3) to calculate ψ-nucleon total cross sections from reported values of $d\sigma/dt$ at $t = 0$, neglecting the real part of the forward-scattering amplitude and using the lepton-pair partial width $\Gamma_{ee} = 4.8$ keV (43). These values are shown in Figure 13 as a function of c.m. energy. The experiment of Camerini et al (45) has provided a direct measurement of the ψ-nucleon cross section, inferred from the ratio of yields in Be and Ta. From results with 20-GeV incident photons, they find $\sigma(\psi N) = 2.8 \pm 0.9$ mb, where only statistical errors are included in the uncertainty. The systematic error was estimated at $\sim \pm 0.5$ mb. The first directly measured ψ-interaction cross section agrees with values extracted from the photoproduction cross sections with vector-dominance model.

It appears that the ψN total cross section approaches a value $\sigma \simeq 1$ mb, small, but within the range typical of strong-interaction processes. It is noteworthy that

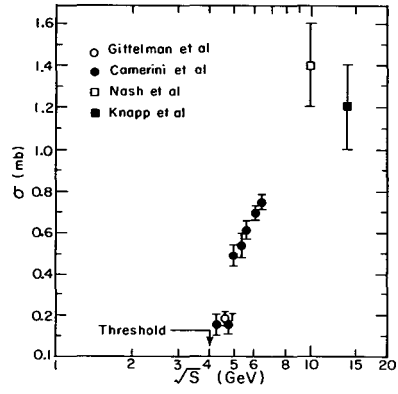

Figure 13 Compendium of results on the energy dependence of the ψ(3095)-nucleon total-interaction cross section obtained from photoproduction data of (44–48) and the vector-dominance model.

this ψ-nucleon cross section is smaller by a factor of ten than the ϕ-nucleon total cross section. Also the energy dependence has a shape somewhat suggestive of a threshold for an inelastic ψ-nucleon reaction at an energy near 5 GeV in the ψ-nucleon c.m. system. Candidates for such reactions are the processes yielding pairs of charmed mesons, implicit in the four-quark view of hadron microstructure.

The yield of ψ' in photoproduction is considerably smaller than that of ψ. Only Camerini et al (45) report a positive result. With 21-GeV photons, they measure $d\sigma/dt = (2.1 \pm 0.8) \times 10^{-33}$ cm^2 (GeV/c)$^{-2}$ at minimum momentum transfer, just about one seventh of the value for ψ photoproduction at the same energy and its minimum momentum transfer.

3 PROPERTIES OF ψ(3095) AND ψ(3684)

Essentially all information on the characteristics of the resonant states has come from analysis of e^+e^- annihilations and mostly from the SLAC-LBL group at SPEAR and the Double Arm Spectrometer (DASP) group at DORIS (27). The LBL-SLAC magnetic detector (49) is a cylindrical arrangement of counters and spark chambers arrayed around the direction of the colliding beams as the axis, all in an axial magnetic field of $\sim$4000 G uniform to a few percent over its $\sim$3-m-diameter-by-$\sim$3-m-length volume. Charged particles and photons are detected over about 65% of the full solid angle. A schematic view of a vertical cross section through the detector axis is shown in Figure 14. The DASP apparatus (50), Figure 15, is a symmetric pair of magnetic spectrometers providing precise momentum and time-of-flight measurements of charged particles produced in a solid angle of $\sim 0.1 \times 4\pi$ sr. The nonmagnetic inner detector covers $\sim 0.7 \times 4\pi$ sr. Both the SLAC-LBL and DASP apparatuses detect photons, DASP with better efficiency, energy, and position resolution.

3.1 *Masses and Widths*

The resonant-state energies, full widths, and partial widths were determined from data obtained at SPEAR on the energy dependence of the annihilation cross section shown in Figures 5 and 6 (43, 51). For these data the incident flux was obtained from measurement of Bhabha scattering at ~ 25 mrad. Hadron yields were corrected for the solid-angle and momentum acceptance of the apparatus, using a Monte Carlo simulation of the detector response and a phase-space production model (52). That calculation yields a net detection efficiency $\varepsilon = 0.4$ with $\pm 15\%$ estimated uncertainty. Lepton-pair cross sections refer only to the angular range $|\cos\theta| \leqq 0.6$, where θ is the angle between the final-state leptons' and initial

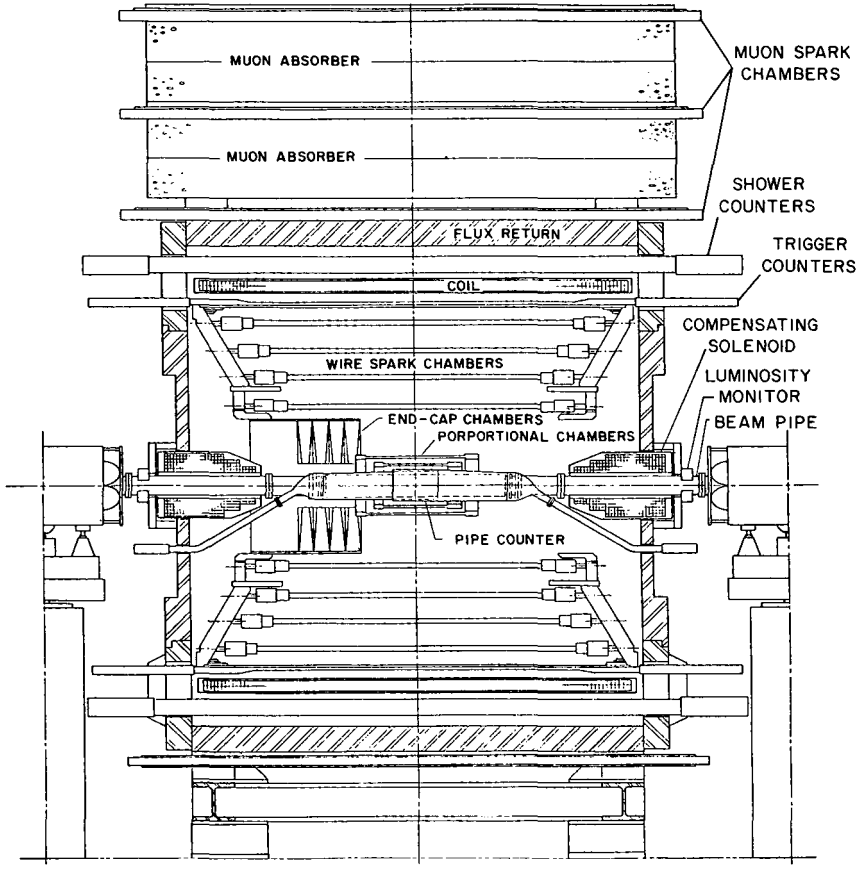

Figure 14 The SLAC-LBL magnetic detector at the e^+e^- storage ring SPEAR; a view in the vertical plane through the intersecting beams.

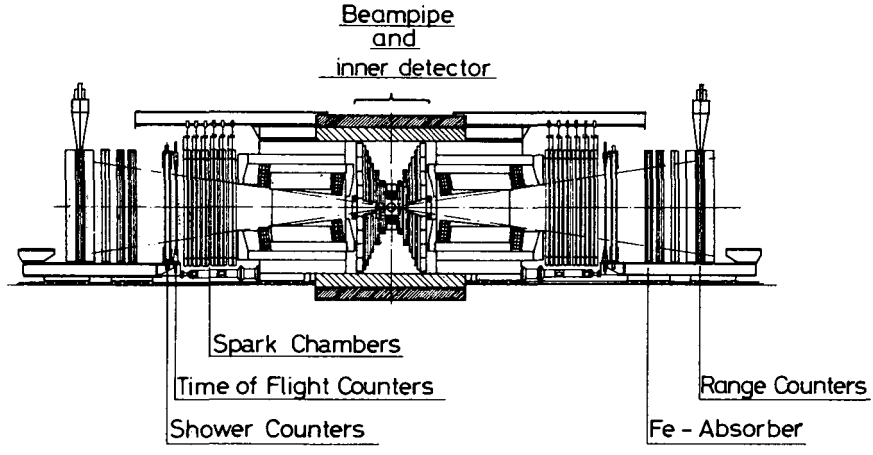

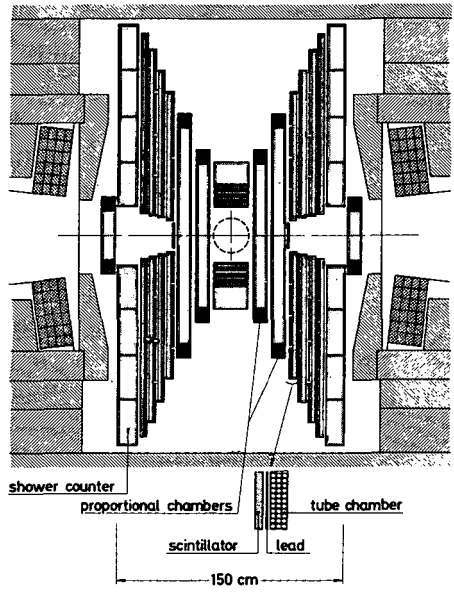

DASP — Inner Detector

Figure 15 The Double Arm Spectrometer detector (DASP) at the e^+e^- storage rings DORIS.

Table 3 Parameters of ψ particles

Particle	Mass (MeV/c^2)	Γ (MeV)	Γ_{ee} (keV)	$\Gamma_{\mu\mu}$ (keV)	Γ_h (keV)	$\Gamma_{\gamma h}$ (keV)	$f_v^2/4\pi$
$\psi(3095)$[a]	3095 ± 4	0.069 ± 0.015	4.8 ± 0.6	4.8 ± 0.6	59 ± 15	12 ± 2	11.5 ± 1.4
$\psi(3684)$[b]	3684 ± 5	0.228 ± 0.056	2.1 ± 0.3	2.1 ± 0.3	224 ± 56	7 ± 1	31.1 ± 4.5
$\psi(4414)$[c]	4414 ± 7	33 ± 10.0	0.44 ± 0.14				178 ± 57

[a] LBL-SLAC values (43).
[b] LBL-SLAC values (51).
[c] Reference 101.

beams' directions. The observed excitation curves were each fit to a function consisting of a Breit-Wigner line shape for a resonance at energy M of full width Γ,

$$\sigma_\beta(W) = \frac{(2J+1)\pi}{W^2} \frac{\Gamma_{ee}\Gamma_\beta}{(W-M)^2 + \Gamma^2/4}, \tag{3.1}$$

convoluted with the energy-resolution function of the colliding beams. The parameters Γ_{ee} and Γ_β are the partial widths for decays to electron pairs and final state β, respectively. The observed cross section at nominal interaction energy W_0 (the storage-ring energy setting) is then

$$\sigma_\beta(W_0) = \int G_R(W_0 - W)\sigma_\beta(W)\, dW, \tag{3.2}$$

where initial-state radiation has been taken into account by replacing the resolution function $G(W_0 - W)$ by a radiatively corrected form (53)

$$G_R(W_0 - W) = t \int_0^{W_0/2} \left(\frac{2k}{W_0}\right)^t G(W_0 - W - k) \frac{dk}{k}, \tag{3.3}$$

where $t = 2(\alpha/\pi)[\ln(W_0/M_e)^2 - 1]$ and k is the energy of a radiated photon. Radiation causes a "tail" on the high-energy side of a resonance, decreasing the maximum observed cross section, but does not appreciably change the position of the maximum. Best-fit values obtained for M, Γ, Γ_{ee}, $\Gamma_{\mu\mu}$, and Γ_h, the hadron width, are listed in Table 3. It was assumed that no decay modes escaped detection, i.e. $\Gamma = \Gamma_h + \Gamma_{\mu\mu} + \Gamma_{ee}$. It is of some value to note here the more transparent relation between the resonance parameters and the area under the resonance peak

$$\int\int \sigma_\beta(W_0) G(W_0 - W)\, dW\, dW_0 = \frac{2\pi^2}{M^2}(2J+1)\frac{\Gamma_{ee}\Gamma_\beta}{\Gamma}, \tag{3.4}$$

independent of the shape of the resolution function. Assuming no modes escape detection, the sum of the areas under the three resonance peaks shown determines the electron-pair partial width directly.

Included in Γ_h is a contribution $\Gamma_{\gamma h}$, from resonance decays via a second-order electromagnetic process, indicated in Figure 16*b*. With the usual assumption that

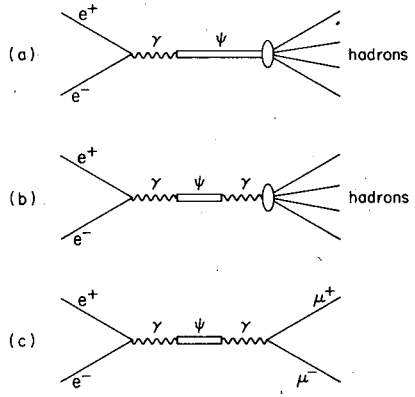

Figure 16 Diagrams of resonance production in lowest order in e^+e^- annihilation with decays to (*a*) hadrons, (*b*) hadrons via second-order electromagnetic interaction, and (*c*) muon pairs.

lepton pairs couple to the resonant state via an intermediate photon, it follows

$$\Gamma_{\gamma h} = \left[\frac{\sigma(e^+e^- \to \text{hadrons})}{\sigma(e^+e^- \to \mu^+\mu^-)}\right]\Gamma_{\mu\mu},$$

where the quantity in brackets is evaluated at an energy just below resonance. Values of the cross-section ratio measured by the SLAC-LBL group (52) were used to calculate the second-order electromagnetic widths given in the table. The fraction of indirect hadronic decays, $\Gamma_{\gamma h}/\Gamma$, is 0.17 ± 0.03 for $\psi(3095)$ and 0.031 ± 0.009 for $\psi(3684)$.

3.2 *Spin, Parity, and Charge Conjugation*

These quantum numbers are directly established to have values $J = 1$, $P =$ odd, and $C =$ odd from the observation of interference between single-photon–exchange and ψ-exchange amplitudes in the process $e^+e^- \to$ leptons near resonance, Figure 16*c* (43, 51). If the intermediate meson has the same quantum numbers as the photon, the muon-pair-annihilation differential cross section is

$$\frac{d\sigma}{d\Omega} = \frac{9}{16W^2}(1+\cos^2\theta)\left|\frac{-2\alpha}{3} + \frac{\Gamma_{\mu\mu}}{M - W - i\Gamma/2}\right|^2,$$

showing destructive interference below the resonant energy M. To minimize the effects of uncertainties in incident-flux determinations, the SLAC-LBL group examined the ratio of electron-pair to muon-pair cross sections, integrated over the angular interval $-0.6 < \cos\theta < 0.6$ covered by the detector. That ratio is shown as a function of energy in Figure 17, together with calculated curves, due account having been taken of radiative corrections. Both $\psi(3095)$ and $\psi(3684)$ data are consistent with expectations for spin-1 and exclude spin-0. Interference observations directly establish that both psions and the photon have the same value, -1,

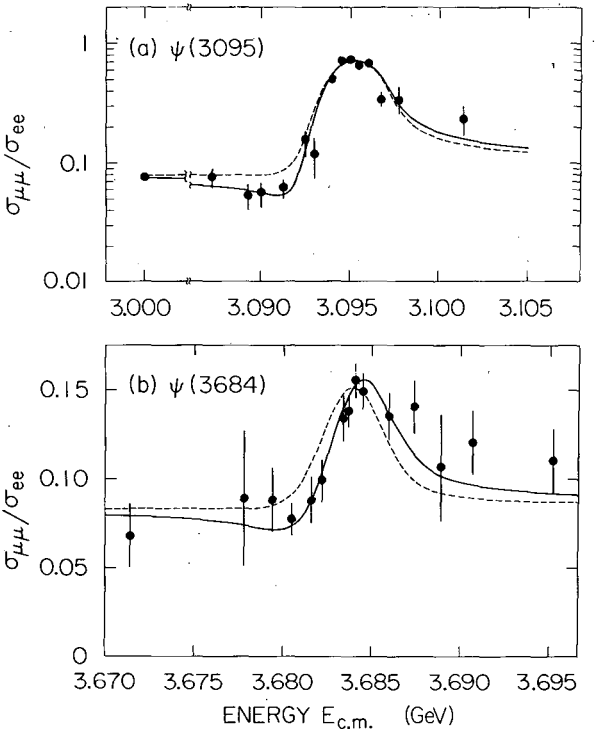

Figure 17 Ratio of cross sections for e^+e^- annihilation to muon pairs to that for annihilation to electron pairs at energies near (*a*) 3095 MeV and (*b*) 3684 MeV. The full and dashed curves show maximal and zero interference, respectively, between one photon and resonance amplitudes; from LBL-SLAC (43, 51).

of parity and charge-conjugation quantum numbers. Spin greater than one is not excluded a fortiori by an interference observation because the unit helicity projection of the intermediate ψ will produce interference effects in the energy variation of that fraction of the total cross section included in the limited angular range of detection. Since the QED amplitude is nonzero only for transitions between lepton-pair states of helicity ± 1, the interference term in the cross section is proportional to the overlap integral of the spin-rotation functions $d^J_{11}(\theta)$ and $d^1_{11}(\theta)$. It follows from the properties of the $d^J_{11}(\theta)$ functions that ψ-spin values two and three give rise to constructive interference at energies below resonance. Higher spins produce negligible interference. Spins greater than, as well as less than, one are thus excluded by the LBL-SLAC data.

3.3 *Hadronic Decays of ψ(3095); Isospin and G-Parity; SU(3) Classification*

Table 4 presents information on hadronic-decay modes of $\psi(3095)$.

Table 4 Branching fractions for $\psi(3095)$ nonleptonic decays

Mode	Fraction (%)[a]	Ref.	Footnote(s)
$\pi^+\pi^-$	0.01 ± 0.007	54	b
$\pi^+\pi^-\pi^0$	1.6 ± 0.6	55	—
$\rho\pi$	1.3 ± 0.2	54, 55	c
$2\pi^+2\pi^-$	0.4 ± 0.1	55	d
$\pi^\pm A_2^\mp$	<0.4	54	d
$2\pi^+2\pi^-\pi^0$	4 ± 1	55	—
$\omega\pi^+\pi^-$	0.7 ± 0.2	57	e
ωf	0.19 ± 0.08	57	e
ρA_2	0.8 ± 0.5	57	e
$\rho\pi\pi\pi$	1.2 ± 0.4	55	e
$3\pi^+3\pi^-$	0.4 ± 0.2	55	d
$3\pi^+3\pi^-\pi^0$	2.9 ± 0.7	55	—
$\omega 2\pi^+2\pi^-$	0.9 ± 0.3	57	f
$4\pi^+4\pi^-\pi^0$	0.9 ± 0.3	55	—
K^+K^-	0.02 ± 0.02	57	g
$K_S^0K_L^0$	<0.008	57	g
$K_S^0K^\pm\pi^\mp$	0.26 ± 0.07	57	—
$K^0\bar{K}^{*0}$	0.27 ± 0.06	57	h, i, j
$K^\pm K^{*\mp}$	0.32 ± 0.06	57	h, j
$K^0\bar{K}^{**0}$	<0.2	57	h, i, j
$K^\pm K^{**\mp}$	<0.15	57	h, j
$K^+K^-\pi^+\pi^-$	0.7 ± 0.2	57	—
$K^{*0}\bar{K}^{*0}$	<0.05	57	g, h, k
$K^{*0}\bar{K}^{**0}$	0.7 ± 0.3	57	h, i, k
$K^{**0}\bar{K}^{**0}$	<0.3	57	g, h, k
$\phi\pi^+\pi^-$	0.14 ± 0.06	57	k
ϕf	<0.04	57	—
$K^+K^-K^+K^-$	0.07 ± 0.03	57	—
ϕK^+K^-	0.09 ± 0.04	57	l
$\phi f'$	0.08 ± 0.05	57	l
$K^+K^-\pi^+\pi^-\pi^0$	1.2 ± 0.3	57	—
ωK^+K^-	0.08 ± 0.05	57	m
$\omega f'$	<0.02	57	m
$\phi\eta$	0.10 ± 0.06	57	m
$\phi\eta'$	<0.1	57	—
$K^+K^-2\pi^+2\pi^-$	0.3 ± 0.1	57	n
$\phi 2\pi^+2\pi^-$	<0.15	57	—
$\bar{p}p$	0.22 ± 0.02	54, 56	o
$\bar{N}N\pi$	0.4 ± 0.2	56	p
$\Lambda\bar{\Lambda}$	0.16 ± 0.08	56	o
$\gamma\gamma$	<0.05	74	q
$\gamma\pi^0$	<0.055	74	—
$\gamma\eta$	0.14 ± 0.04	50, 73	—
$\gamma\eta'$	<0.7	50, 73	—
$\gamma X(2800)$	<1.7	68	—
$\gamma X(\rightarrow 3\gamma)$	~ 0.015	50, 73	—

Table 4 Continued

[a] All upper limits refer to the 90% confidence level.
[b] Two events detected with background estimated at 0.24 events. An isospin-nonconserving, second-order electromagnetic mode.
[c] $\rho^0\pi^0 + \rho^\pm\pi^\mp$. Included in $\pi^+\pi^-\pi^0$ grouping.
[d] Proceeds via second-order electromagnetic interaction.
[e] One-π^0 mode included in $2\pi^+2\pi^-\pi^0$.
[f] One-π^0 mode included in $3\pi^+3\pi^-\pi^0$.
[g] Forbidden for SU(3) singlet.
[h] $K^* \equiv K^*(892)$, $K^{**} \equiv K^*(1420)$.
[i] Includes charge-conjugate state.
[j] $K_S^0K^\pm\pi^\mp$ fraction included in $K_S^0K^\pm\pi^\mp$ grouping.
[k] $K^+K^-\pi^+\pi^-$ fraction included in $K^+K^-\pi^-\pi^-$ grouping.
[l] $K^+K^-K^+K^-$ fraction included in $K^+K^-K^+K^-$ grouping.
[m] $K^+K^-\pi^+\pi^-\pi^0$ fraction included in $K^+K^-\pi^+\pi^-\pi^0$ grouping.
[n] $K^+K^-2\pi^+2\pi^-$ fraction included in $K^+K^-2\pi^+2\pi^-$ grouping.
[o] Angular distribution $1 + \cos^2\theta$ assumed, consistent with data.
[p] Includes $p\bar{p}\pi^0$, $p\bar{n}\pi^-$, and $n\bar{p}\pi^+$.
[q] Forbidden for angular momentum $J = 1$.

Two-body branching ratios have been determined by Braunschweig et al (54) from data obtained with the double arm spectrometer DASP. Two-body final states were selected, using criteria of collinearity, momentum, energy loss, and range appropriate to the particular pair. Evidence for the modes $\pi^\pm\rho^\mp$ and $K^\pm K^{*\mp}$ is presented in the missing-mass spectra of Figure 18, showing the mass recoiling against single pions and kaons.

Multibody decay rates were measured by the SLAC-LBL group (55–57) using kinematical fits of multiprong events in which the detected prongs have zero total charge. Events with no missing particles were selected by requiring that the missing momentum be less than 100 MeV/c. As an example, the distribution in total energy of the detected prongs in four-prong events is shown in Figure 19. Four-particle

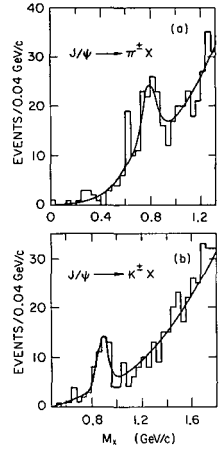

Figure 18 Distribution of mass recoiling against (*a*) single pions and (*b*) single kaons in multihadron decays of $\psi(3095)$ produced in e^+e^- annihilations; from DASP (54).

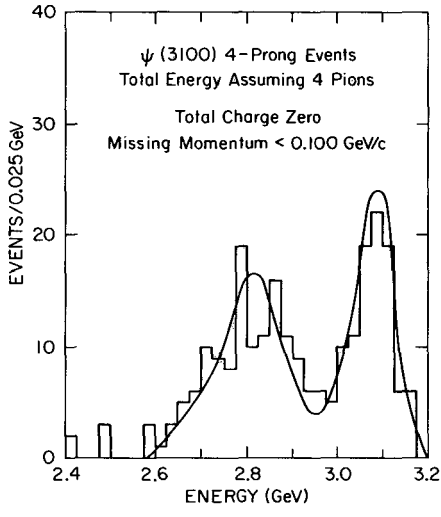

Figure 19 Total energy in four-prong $\psi(3095)$ decay events with missing momentum less than 100 MeV/c. The solid curve is a Monte Carlo fit to the data; from SLAC-LBL (55, 56).

states, presumed to be $\pi^+\pi^-\pi^+\pi^-$, are indicated by the presence of the peak near 3100 MeV in total detected energy. Events with momentum unbalance greater than 200 MeV/c exhibit the missing-mass spectrum of Figure 20 with clear evidence for the $2\pi^+2\pi^-\pi^0$ decay mode of the ψ and, for contrast, its relative absence at the nonresonant energy 3.0 GeV. Similar analysis techniques were used by the LBL-SLAC group to identify samples of the various final states of Table 4 and, after correction for losses due to detection inefficiency, to determine the branching ratios shown.

Application of these results to the determination of strong-interaction properties of the ψ requires isolation of the direct-decay contribution (Figure 16*a*) from that of the second-order electromagnetic decays (Figure 16*b*). That is done by comparing the relative branching ratio $\sigma_\beta/\sigma_{\mu\mu}$ for a final state β at resonance to the same quantity at 3.0 GeV, where the resonance contribution is negligible. Jean-Marie et al (55) show that this ratio, measured at resonance, equals the nonresonant value for states with even numbers of pions. States with odd numbers of pions have significantly larger cross-section ratios at resonance than below resonance, leading to the conclusion that ψ couples directly to states with odd numbers of pions and not to states with even numbers of pions. It follows that the ψ is a hadronic state of odd G-parity. Applying the relation between isospin and G-parity for a state of arbitrary number of pions,

$$G = C(-1)^I = (-1)^{I+1}$$

it follows that the ψ is a state of even isospin and that direct decays of the ψ follow the hadronic rule of isospin conservation.

The $\pi^+\pi^-\pi^0$ event class of Jean-Marie et al (55) is dominated by the quasi-two-body $\rho\pi$ state, as indicated in the Dalitz plot of Figure 21. From the distribution of events, they concluded that for ψ decay,

$$\frac{\Gamma_{\rho^0\pi^0}}{\Gamma_{\rho^+\pi^-}+\Gamma_{\rho^-\pi^+}} = 0.59 \pm 0.17.$$

Comparison with the values 0.5 and 2.0, appropriate to isospin-conserving decays of objects of isospin zero and two, respectively, uniquely establishes $I = 0$ for the ψ. Confirmation of this result came with observation of the $\bar{p}p$ mode by the DASP and LBL-SLAC groups. As pointed out by Braunschweig et al (54), the measured ratio $\Gamma_{\bar{p}p}/\Gamma_{\mu\mu}$ is much larger than would be obtained with any plausible extrapolation of the nucleon form factor, so that the $\bar{p}p$ mode must represent a direct decay, rather than a second-order electromagnetic process. That state can occur only with $I = 0$ or $I = 1$, and the latter is excluded by inference from the existence of decays to odd numbers of pions. Lastly, the LBL-SLAC team has reported a

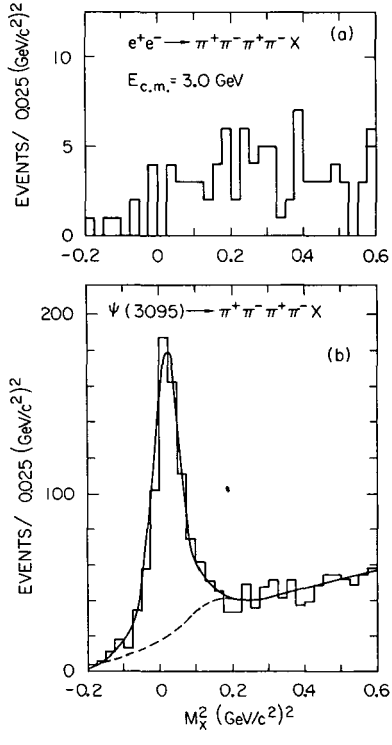

Figure 20 Missing mass-squared in four-prong events with missing momentum greater than 200 MeV/c produced in e^+e^- annihilations at (*a*) 3.0 GeV and (*b*) $\psi(3095)$ resonance. The solid curve is a Monte Carlo fit to the data; from LBL-SLAC (55, 56).

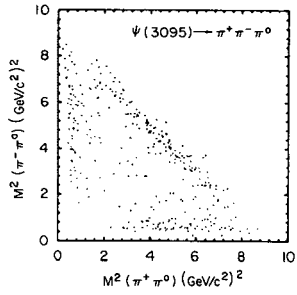

Figure 21 Dalitz plot for $\psi(3095)$ decays to $\pi^+\pi^-\pi^0$; from SLAC-LBL (55, 56).

measurement of the $\Lambda\bar{\Lambda}$ branching ratio, $\Gamma_{\Lambda\bar{\Lambda}}/\Gamma = 0.0016 \pm 0.0008$, based on twenty well-identified examples (56). None of those is consistent with primary $\Sigma^0\bar{\Lambda}^0$ ($\bar{\Sigma}^0\Lambda^0$) events. Since second-order electromagnetic decays populate $\Sigma\bar{\Lambda}$ states six times more frequently than $\Lambda\bar{\Lambda}$ states (58), it follows that the $\Lambda\bar{\Lambda}$ pairs are direct decay products. This observation provides another argument for assigning $I = 0$ to the $\psi(3095)$.

Two-body-decay branching ratios are especially useful in considering the applicability to ψ-decay interactions of the broader SU(3) strong-interaction symmetry (58, 59). Decay of an SU(3) singlet is constrained severely because only one amplitude determines the rates for all decays $\psi \to m_a + m_b$, where m_a and m_b represent any two members of meson octets. If m_a and m_b are the charged members of an $I = 1$ submultiplet, $m_a + m_b$ has even G-parity and is not an allowed final state for $\psi(3095)$ decay. By extension, decay to any two members of the same octet is forbidden. If m_a and m_b are the $I = 1$, $I_3 = 0$, $Y = 0$ members of different octets, a and b, and the charge-conjugation quantum numbers of m_a and m_b are equal, then m_a and m_b have the same G-parity, so the state $m_a + m_b$ also has even G-parity. Decay of an odd G-parity, SU(3) singlet to that state is again forbidden. Symmetry under SU(3) then forbids $\psi(3095)$ decay to a state of any two members of such octets a and b. Allowed decay modes are, for example, $\rho\pi$, $\eta\phi$, and $\bar{K}K^*(890)$, while K^+K^-, πA_2, $\bar{K}K^*(1420)$ are forbidden. Inspection of the branching fractions listed in Table 4 shows that the SU(3)-singlet-allowed modes $K\bar{K}^*(890)$ and $K^*(890)\bar{K}^*(1420)$ occur, and with branching fractions at least an order of magnitude larger than those for $\pi^+\pi^-$ and K^+K^-. Other forbidden modes, $\bar{K}K^*(1420)$, $K^*\bar{K}^*$, etc have not appeared, but present upper limits on their relative rates are not very convincingly small.

Exact SU(3) symmetry leads to the further prediction of equal branching ratios for allowed singlet decays to any two members, m_a and m_b, of any pair of octets a and b, e.g. to $\pi^0\rho^0$, $\pi^+\rho^-$, $\pi^-\rho^+$, $K^-K^{*+}(892)$, $K^+K^{*-}(892)$ etc. The relevant experimental ratios are

$$[\Gamma(\pi^+\rho^-)+\Gamma(\pi^-\rho^+)+\Gamma(\pi^0\rho^0)]/[\Gamma(K^+K^{*-})+\Gamma(K^-K^{*+})]/[\Gamma(K^0\bar{K}^{*0}) + \Gamma(\bar{K}^0K^{*0})] = (1.3 \pm 0.2)/(0.34 \pm 0.06)/(0.27 \pm 0.05),$$

not quite in agreement with the predicted 3/2/2, indicating some SU(3) breaking in the decay interaction.

In summary, ψ decays appear to have properties in agreement with the strictures of SU(3) symmetry appropriate to a singlet state, although there are some discrepancies.

3.4 *Hadronic Decays of $\psi(3684)$; Isospin and G-Parity*

The dominant hadronic decay mode of $\psi(3684)$ is the cascade decay to $\psi(3095)$, $\psi' \to \psi\pi\pi$. The modes $\psi\pi^+\pi^-$, $\psi\pi^0\pi^0$, together with $\psi' \to \psi\eta$ and $\psi' \to \psi\gamma\gamma$, account for just over one-half of all decays. Table 5 lists branching ratios for all identified hadronic modes. Data from the DASP (50) and LBL-SLAC (60, 61) groups were obtained using the detection apparatus and analysis techniques described above. Hilger et al (62), at SPEAR, used two identical collinear spectrometers, each equipped with a large NaI crystal for photon and electron detection, an array of multiwire proportional chambers for track-trajectory sampling, and a magnetized iron block

Table 5 Branching fractions for $\psi(3684)$ nonleptonic decays

Mode	Fraction (%)[a]	Ref.	Footnote(s)
$\psi(3095)\pi^+\pi^-$	33 ± 3	50, 60–62	—
$\psi\pi^0\pi^0$	17 ± 3	50, 60–62	—
$\psi\eta$	4.2 ± 0.7	50, 61	—
$\psi\gamma + \psi\pi^0$	< 0.15	61	b, c
$\pi^+\pi^-$	< 0.04	54	d
$2\pi^+2\pi^-\pi^0$	0.35 ± 0.15	56	—
$\rho^0\pi^0$	< 0.1	56	—
K^+K^-	< 0.14	54	e
$p\bar{p}$	< 0.05	54	f
$\gamma\gamma$	< 0.5	69	g
$\gamma\pi^0$	< 0.7	69	—
$\gamma\eta$	< 0.13	50	—
$\gamma X(2800)$	< 1	65, 68	—
$\gamma X(2800) \to 3\gamma$	< 0.04	50	—
$\gamma\chi(3415)$	7 ± 2	65, 68	f
$\gamma\chi(3510)$	7 ± 2	68	h
$\gamma\chi(3550)$	7 ± 2	68	h
$\gamma\chi(3455)$	< 2.5	68	—
$\gamma\chi(3455) \to \gamma\gamma\psi$	0.8 ± 0.4	65	—

[a] All upper limits refer to the 90% confidence level.
[b] $\psi\gamma$ forbidden by c invariance.
[c] $\psi\pi^0$ forbidden by isospin invariance.
[d] Isospin-nonconserving, second-order electromagnetic decay.
[e] Forbidden for an SU(3) singlet.
[f] Angular distribution $1 + \cos^2\theta$ assumed.
[g] Forbidden for angular momentum 1.
[h] Isotropic angular distribution assumed. With $1 + \cos^2\theta$ distribution, these branching fractions increase by a factor of 1.3.

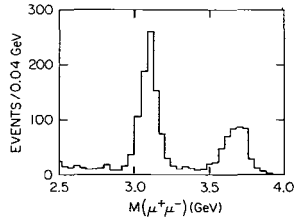

Figure 22 Inclusive distribution of muon-pair invariant masses from $\psi(3684)$ decays showing evidence of cascade decays to $\psi(3095)$; from LBL-SLAC (60).

for charged-particle momentum determination. The spectrometers were perpendicular to the direction of the colliding beams.

The LBL-SLAC evidence for the cascade decay $\psi(3684) \rightarrow \psi(3095) +$ anything (60) is presented in Figure 22. This shows the distribution in invariant mass of the two highest-momentum, oppositely charged prongs in the $\psi(3684)$ decays, calculated with the muon mass assumed for those two tracks. A peak at the ψ mass is apparent, as is the peak at 3684 MeV/c^2, due to direct decays of $\psi(3684)$ to muon pairs. Figure 23*a* shows the mass recoiling against all $\pi^+\pi^-$ pairs in all events, exhibiting again a clear peak at 3095 MeV/c^2. Figure 23*b* shows the recoil mass against those pion pairs in 4-prong events with zero total charge and, within experimental uncertainties, zero missing momentum, consistent with kinematics of the decay $\psi(3684) \rightarrow \mu^+\mu^-\pi^+\pi^-$. The peak results from that subset of $\psi(3684)$ cascade decays in which $\psi(3095)$ subsequently decays via its muon-pair mode. An example of a computer reconstruction of such an event is shown in Figure 24. The SLAC-LBL group identified $\psi' \rightarrow \psi\eta$ decays among the class of $\pi^+\pi^-\mu^+\mu^-$ events with missing momentum (61). The distribution in the square of the mass recoiling against the $\mu^+\mu^-$ pairs in Figure 25 shows a peak at the $\eta(\text{mass})^2$ whose

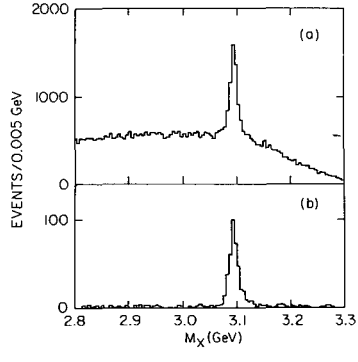

Figure 23 (*a*) Distribution of missing mass recoiling against all pairs of oppositely charged particles in $\psi(3684)$ decays to multihadron states. (*b*) same as (*a*), but for events consistent with zero missing energy and momentum; from SLAC-LBL (60).

width is consistent with that expected from experimental resolution folded with the natural width of the η meson. The $\psi\eta$ mode is also revealed in the LBL-SLAC group's mass spectrum of all-neutral states accompanying ψ decays via the $\mu^+\mu^-$

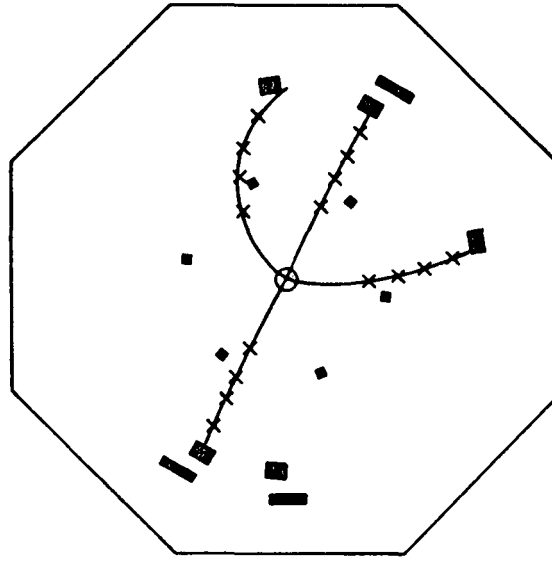

Figure 24 A computer reconstruction of a $\psi(3684) \to \pi^+\pi^-\psi(3095) \to \pi^+\pi^-e^+e^-$ event in the LBL-SLAC detector seen in projection on the plane perpendicular to the intersecting beams. The ×'s mark spark-chamber samplings. Black rectangles show counters. The straightest two tracks are the electron and positron; the others are the low-momentum pions; from SLAC-LBL (60).

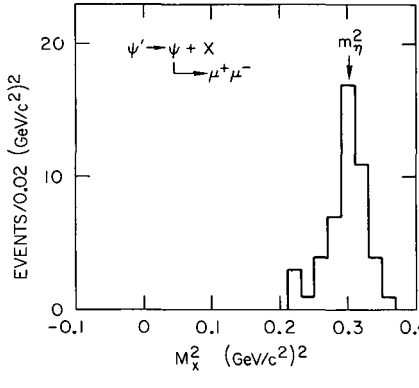

Figure 25 Distribution of square of recoil mass accompanying $\psi(3095)$-decay muons in $\psi' \to \psi\pi^+\pi^- \to \mu^+\mu^-\pi^+\pi^-$ events not consistent with kinematics of $\psi(3684) \to \psi(3095)\pi^+\pi^-$ decay; from LBL-SLAC (61).

mode. Figure 26 shows the spectrum of missing mass-squared in events of the type $\psi' \to \mu^+\mu^- +$ neutrals, with a clear η peak. This is particularly prominent after subtracting a calculated contribution to the data expected from $\psi' \to \pi^0\pi^0\psi \to \pi^0\pi^0\mu^+\mu^-$, using the isospin-conservation prediction $\pi^0\pi^0/\pi^+\pi^- = \frac{1}{2}$ for a $\pi\pi$ system of zero isospin and the measured rate for $\psi' \to \psi\pi^+\pi^-$. Subsequently, direct observation was made by the DASP group of the decay $\psi' \to \psi\pi^0\pi^0$ (50), examples of which were reconstructed from events with ψ-decay muon pairs and detected γ rays. They measured a branching ratio

$$\Gamma(\psi' \to \psi\pi^0\pi^0)/\Gamma = 0.18 \pm 0.06.$$

The yield of events with muon pairs and charged particles provided data for their determination of the branching ratio

$$\Gamma(\psi' \to \psi\pi^+\pi^-)/\Gamma = 0.36 \pm 0.06,$$

in good agreement with the LBL-SLAC value 0.32 ± 0.04. The LBL-SLAC results yielded

$$\Gamma(\psi' \to \psi\pi^0\pi^0)/\Gamma = 0.17 \pm 0.04,$$

upon subtraction of the $\psi\eta$ (61) and $\psi\gamma\gamma$ (63) branching fractions from the directly measured value

$$\Gamma(\psi' \to \psi + \text{neutrals})/\Gamma = 0.25 \pm 0.04.$$

The LBL-SLAC and DASP values are in good agreement. Weighted averages are listed in Table 5, which summarizes the available data.

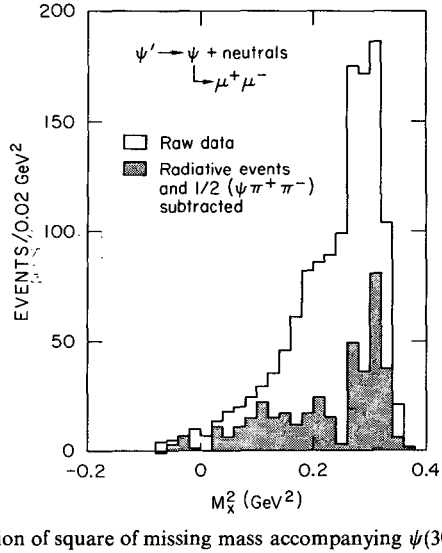

Figure 26 Distribution of square of missing mass accompanying $\psi(3095)$-decay muons in events containing $\mu^+\mu^-$ and undetected neutral particles; from SLAC-LBL (61).

Branching ratios to other exclusive hadronic states are relatively small. Comparison of the rates for ψ decay in Table 4 with those for ψ' in Table 5 reveals strong differences in the various branching ratios. In particular, the $\pi^+\pi^-\pi^+\pi^-\pi^0$ mode, prominent in $\psi(3095)$ decay, has a branching ratio smaller by an order of magnitude in $\psi(3684)$ decay.

Assignment of odd G-parity to $\psi(3684)$ follows directly from the existence of the $\psi\pi\pi$ mode and the value $G = -1$ for $\psi(3095)$ previously established.

Isospin is determined from the ratio of partial widths

$$\Gamma(\psi' \to \psi\pi^0\pi^0)/\Gamma(\psi' \to \psi\pi^+\pi^-)$$

which, corrected for the difference between the $\pi^+\pi^-$ and $\pi^0\pi^0$ phase space, has the predicted value 0.52 for $I = 0$, zero for $I = 1$, and 2.1 for $I = 2$. The measured value is

$$\Gamma(\psi' \to \psi\pi^0\pi^0)/\Gamma(\psi' \to \psi\pi^+\pi^-) = 0.5 \pm 0.1,$$

based on the combined results of the LBL-SLAC and DASP experiments. That conclusion appears to be consistent with the measurement of Hilger et al (62) of

$$\Gamma(\psi' \to \psi + \text{neutrals})/\Gamma(\psi' \to \psi\pi^+\pi^-) = 0.64 \pm 0.15,$$

considering that there is some unevaluated contribution from the $\psi\eta$ and $\psi\gamma\gamma$ modes to the ψ + neutrals inclusive rate. Isospin conservation and the isosinglet character of ψ', as well as ψ, is established. This assignment of $I = 0$ is confirmed by the existence of the $\psi' \to \psi\eta$ decay mode.

3.5 *Hadronic Properties of ψ and ψ'*

In summary, the hadronic decays of the psions are characterized by strong-interaction conservation laws for isospin and G-parity. Both $\psi(3095)$ and $\psi(3684)$ have $I = 0$ and $G = -1$. SU(3) appears to be a symmetry of the decay of $\psi(3095)$, and that state has been provisionally classified as a singlet. Cascade to $\psi(3095)$ + pions dominates $\psi(3684)$ decays, with less suppression than other exclusive hadronic modes. These features of the decay dynamics, together with the estimates of $\psi(3095)$ interaction cross sections inferred from photoproduction, establish that the two lightest ψ particles are hadrons.

4 INTERMEDIATE STATES

No resonance peak at any energy between 3095 and 3684 MeV has been found in a series of measurements of e^+e^--annihilation cross sections at small energy intervals (25). Rather, such states have been observed in radiative decay, $\psi' \to \gamma\chi$, of the heavier ψ particle. Those states must thus have even charge-conjugation quantum numbers. The presence of such states has been revealed by the use of three distinct experimental techniques and analysis methods. First, the full cascade-decay chain $\psi' \to \gamma\chi \to \gamma\gamma\psi$ has been observed by detecting the lepton-pair decay products of the ψ with one or two coincident photons. Second, hadronic decay products of χ have been detected. Third, monochromatic photon lines have been observed in the

inclusive energy distribution of photons produced in $\psi(3684)$ decays. For clarity of presentation, we use the generally agreed-upon symbol χ to denote the intermediate states of the psionic system.

4.1 *Cascade Radiative Decays*

Evidence for the existence of intermediate states was first obtained from the study of the $\psi' \to \psi\gamma\gamma$ decays by the DASP group (64) and later corroborated by the LBL-SLAC group (63). Both groups used the $\mu^+\mu^-$ decay mode as a signature of a ψ produced in ψ' decay. In one method of χ-mass determination, used by both groups, two photons were required to have been detected in shower counters. Since the energy resolution is poor, use was made only of the measured photon directions. Those, together with momentum and direction of the ψ, inferred from the $\mu^+\mu^-$ momentum, provided input for a two-constraint fit to the kinematics of the process $\psi' \to \psi\gamma\gamma$. It was estimated that the background from $\psi\pi^0\pi^0$ events is less than 10% of the number of events selected on the basis of quality of the kinematic fit. The DASP group found two clusters of points on a scatter plot of one photon energy versus the other. Since it is not known which of the two photons is the decay product of the χ, each group of photons yields two possible values of χ mass. Using central values of the energies of the two observed groups, they determined the masses to be (3.507 ± 0.007) or (3.258 ± 0.007) GeV/c^2 and (3.407 ± 0.008) or (3.351 ± 0.008) GeV/c^2, with decay widths consistent with zero.

To obtain better resolution in their χ-mass measurements, the LBL-SLAC group used the magnetic detector as a pair spectrometer to measure the energy of photons that had converted in the various pieces of the apparatus preceding the tracking

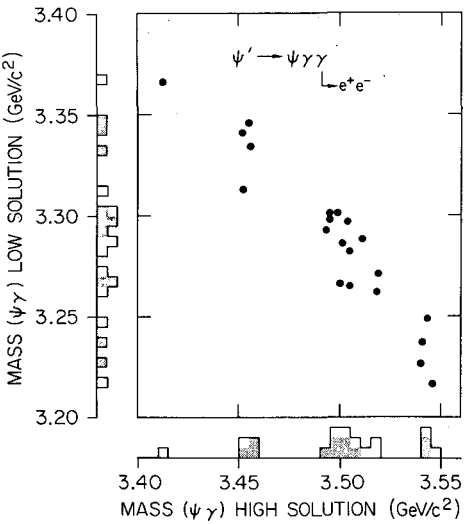

Figure 27 Scatter plot of $\psi\gamma_1$ invariant mass against $\psi\gamma_2$ invariant mass for $\psi(3684)$ decays to $\psi(3095)\gamma_1\gamma_2$; from LBL-SLAC (65).

chambers. The total conversion material has a thickness of some 5% of a radiation length. From an initial sample of 54 events with one converted photon, a subset of $\psi\gamma\gamma$ candidates was selected on the basis of consistency with zero missing mass and indication of the presence of a second photon, revealed by a shower-counter signal. With the elimination of events in which the inferred mass of the photon pair was consistent with the mass of the η, there remain 21 examples of $\psi' \to \psi\gamma\gamma$. One-constraint fits were made to the kinematics of $\psi' \to \psi\gamma\gamma$, in order to obtain values of both photon energies and, for each event, again two values of the mass of the parent of a $\psi\gamma$ pair. These masses are shown plotted against each other in Figure 27 (65). Three clusters are evident, at masses (3543 ± 10), (3504 ± 10), and (3454 ± 10) MeV/c^2. These, rather than the lower-mass alternatives, were chosen as χ masses because the spread of mass around the lower central values is in all cases consistent with that expected from Doppler broadening and the resolution of the apparatus. The one event with $M_\chi \simeq 3415$ MeV/c^2 appears to correspond to the two-event cluster in the DASP results, and the large clumps at $M_\chi = 3504$ MeV/c^2, it is presumed, are to be identified with the DASP events at $M_\chi = 3507$ MeV/c^2.

4.2 *Hadronic Decays of Intermediate States*

Hadronic decays of intermediate states were first identified by Feldman et al (66), who used the LBL-SLAC magnetic detector. Events were restricted to those con-

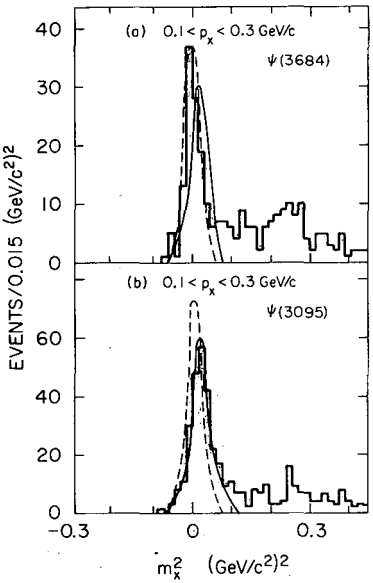

Figure 28 Spectrum of the square of missing mass in four-prong, zero-charge events with missing momentum between 100 and 300 MeV/c for (*a*) $\psi(3095)$ and (*b*) $\psi(3684)$ decays. The solid and dashed smooth curves show calculated resolution functions for a missing π^0 and missing photon, respectively; from SLAC-LBL (66).

taining even numbers of detected particles with total charge zero and momentum unbalance between 100 and 300 MeV/c. This restriction to small missing momentum allows a good separation of events with undetected π^0 from those with undetected photons, based on the observed distribution of missing mass. An example is the missing-mass distribution for the selected four-track events shown in Figure 28, which contrasts the results obtained for the $\psi(3095)$ and $\psi(3684)$ decays. The low-mass peak in the $\psi(3684)$ event sample is consistent with that expected for missing photons and inconsistent with that resulting from undetected neutral pions. Just the opposite conclusion is drawn from the $\psi(3095)$ sample. Adjusted values of particle momenta were obtained from one-constraint fits to the kinematics of $\psi' \to \gamma + \pi^+\pi^-\pi^+\pi^-$ and $\psi' \to \gamma + \pi^+\pi^- K^+K^-$. In subsequent analyses of a larger sample, the SLAC-LBL group used time-of-flight measurements, as well as the quality of the kinematic fit, as criteria for separating events with K^+K^- and $\bar{p}p$ pairs from those

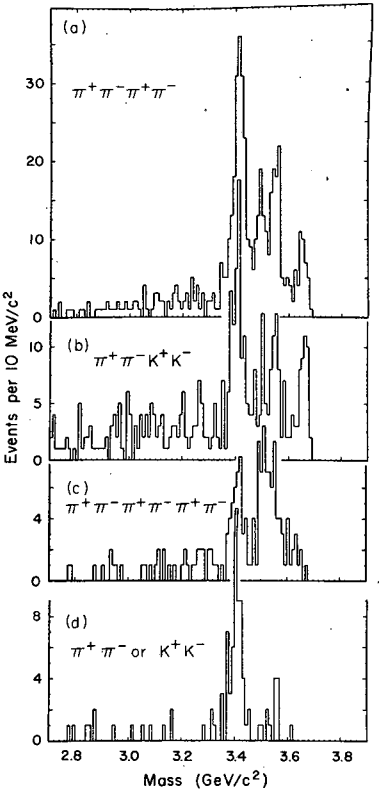

Figure 29 Spectra of invariant masses of states χ fit to the kinematics of the radiative decay $\psi(3684) \to \gamma\chi$ for χ constituent particles identified as indicated in the legends; from LBL-SLAC (67).

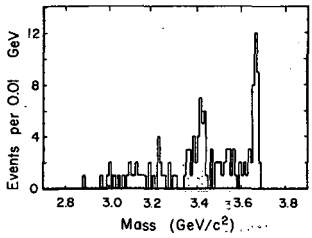

Figure 30 Invariant-mass spectrum of $\pi^+\pi^- p\bar{p}$ products of decays $\psi(3684) \to \gamma\pi^+\pi^- p\bar{p}$ identified with the aid of kinematic fits; from LBL-SLAC (67).

with pions only (67). Similar methods were applied to the analysis of two-prong and six-prong events. Results indicating the presence of decays of distinct states with small decay widths are shown in the mass distributions of Figures 29 and 30. All show prominent peaks at (3415 ± 10) MeV/c^2. Other peaks present at various levels of significance among the spectra are at (3500 ± 10) and (3550 ± 10) MeV/c^2. Noticeably lacking are two-body decays of the state at 3500 MeV/c^2. There is no indication of hadronic decay modes of the proposed state near 3450 MeV/c^2 inferred from results of analysis of the $\psi(3684) \to \psi(3095)\gamma\gamma$ events.

4.3 *Monochromatic Photons*

Certainly, the conceptually simplest and most direct evidence for distinct intermediate states would be the presence of monoenergetic lines in the spectrum of photon-decay products of $\psi(3684)$. Measurements of the yield of photons in the radiative decays of $\psi(3684)$ to the various χ states are essential for the determination of the $\psi' \to \gamma\chi$ and χ decay branching ratios.

The LBL-SLAC group measured the photon-energy spectra using only those photons that had converted to detected electron-positron pairs and whose momenta were then determined from measurements of reconstructed tracks sampled in the track chambers of the detector (65). Energy spectra of photons from $\psi(3684)$ decay and from $\psi(3095)$ are shown in Figure 31. The yield of photons from $\psi(3095)$ decays varies smoothly with photon energy. The shape of the $\psi(3684)$ distribution is similar, but for the evident peak at an energy determined to be (261 ± 10) MeV after correction for energy lost by the electron and positron by ionization. The observed width of the peak is consistent with a true width of zero, broadened by resolution. The inferred mass of the χ state accompanying the photon is (3413 ± 11) MeV/c^2. With appropriate corrections for detection inefficiencies and the assumption of a $1 + \cos^2\theta$ dependence of the photon angular distribution, the LBL-SLAC group finds a branching fraction of 0.075 ± 0.026 for radiative decay to this state. It is reasonably certain that this state is to be identified with the state at (3415 ± 10) MeV/c^2 whose hadronic decays have been observed.

Biddick et al (68) used an arrangement of proportional counters and NaI crystals arrayed about the other interaction region at SPEAR. Superior photon efficiency and energy resolution were achieved with that apparatus. Their results are shown in

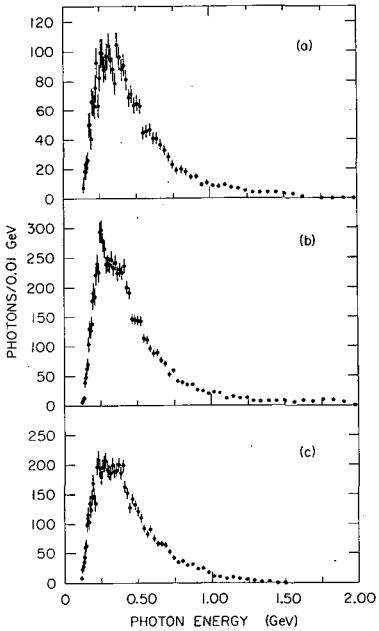

Figure 31 Inclusive energy spectra of photons from decays of (*a*) $\psi(3095)$ and (*b*) $\psi(3684)$; (*c*) a Monte-Carlo-simulated spectrum of π^0 decay photons in multihadron decays of $\psi(3095)$; from SLAC-LBL (67).

Figure 32, containing the spectrum of photons from $\psi(3684)$ decays and, for contrast, that from $\psi(3095)$ decays. In addition to the line at (260.6 ± 2.9) MeV, peaks above the continuum are evident at energies (169.2 ± 1.4) and (120.9 ± 1.3) MeV. The corresponding values of M_χ, 3413, 3511, and 3561 MeV/c^2, may be identified with the states at 3415, 3500, and 3550 MeV/c^2 discussed above, all consistent with the uncertainties in the various mass determinations. Branching ratios obtained by Biddick et al from these yields, corrected for detector acceptance, are

$$\Gamma[\psi' \to \gamma\chi(3415)]/\Gamma(\psi') = 0.072 \pm 0.023,$$

$$\Gamma[\psi' \to \gamma\chi(3510)]/\Gamma(\psi') = 0.071 \pm 0.019,$$

and

$$\Gamma[\psi' \to \gamma\chi(3550)]/\Gamma(\psi') = 0.070 \pm 0.020.$$

The first agrees well with the LBL-SLAC result, to within the substantial errors.

With values of the radiative-decay branching ratios and the branching-ratio products $\Gamma(\psi' \to \gamma\chi)/\Gamma(\psi') \times \Gamma(\chi \to f)/\Gamma(\chi)$ determined from the measured yields corrected for detection inefficiency, we obtain branching fractions for the various

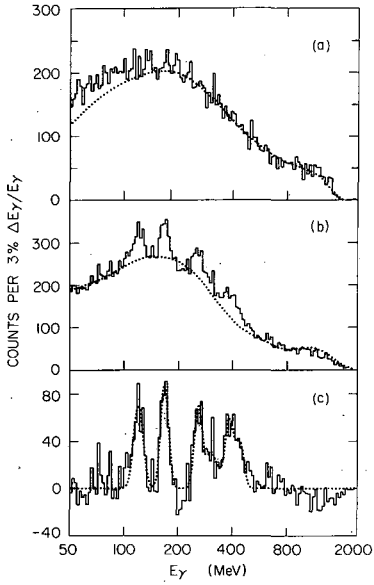

Figure 32 Inclusive energy spectra of photons from (*a*) $\psi(3095)$ and (*b*) $\psi(3684)$; (*c*) continuum subtracted from data of (*b*); from Biddick et al (68) at SPEAR.

detected decay modes of the χ states. The values in Tables 6–8 are to be considered estimates, accurate to approximately a factor of two.

Table 6 Branching fractions for $\chi(3415)$ decays

Mode	Branching fraction (χ) × branching fraction ($\psi' \to \gamma\chi$) (%)	Branching fraction (χ) (%)[a]	Ref.
$\pi^+\pi^-$	0.07 ± 0.02	1.0	67
K^+K^-	0.07 ± 0.02	1.0	67
$\pi^+\pi^-\pi^+\pi^-$	0.32 ± 0.06	4.6	67
$\pi^+\pi^-K^+K^-$	0.27 ± 0.07	3.9	67
$\pi^+\pi^-\bar{p}p$	0.04 ± 0.013	0.6	67
$\pi^+\pi^-\pi^+\pi^-\pi^+\pi^-$	0.14 ± 0.05	2.0	67
$\gamma\psi$	~ 1[b]	14.0	50
	0.2 ± 0.2[c]	3.0	65
	3.3 ± 1.7[d]	47.0	68

[a] Calculated from the branching-ratio product and 0.07 for the $\psi' \to \gamma\chi$ fraction. Estimates, with large uncertainties.
[b] Based on two events.
[c] Based on one event.
[d] Based on a fit to the inclusive energy spectrum of photon-decay products of $\psi(3684)$.

Table 7 Branching fractions for $\chi(3500)$ decay

Mode	Branching fraction (χ) × branching fraction ($\psi' \to \gamma\chi$) (%)	Branching fraction (χ) (%)[a]	Ref.
$\pi^+\pi^-$ and K^+K^-	<0.015	<0.2	67
$\pi^+\pi^-\pi^+\pi^-$	0.11 ± 0.04	1.6	67
$\pi^+\pi^-K^+K^-$	0.06 ± 0.03	0.9	67
$\pi^+\pi^-\bar{p}p$	0.01 ± 0.008	0.1	67
$\pi^+\pi^-\pi^+\pi^-\pi^+\pi^-$	0.17 ± 0.06	2.4	67
$\gamma\psi$	4 ± 2	57	50
	2.4 ± 0.8	34	65
	5.0 ± 1.5[b]	71	68
$\gamma\gamma$[c]	<0.0013	<0.02	50

[a] Calculated from the branching-ratio products and 0.07 for the $\psi' \to \gamma\chi$ fraction. Estimates, with large uncertainties.
[b] Based on a fit to the inclusive energy spectrum of photon decay products of $\psi(3684)$.
[c] Forbidden for spin-1.

Table 8 Branching fractions for $\chi(3550)$ decays

Mode	Branching fraction (χ) × branching fraction ($\psi' \to \gamma\chi$) (%)	Branching fraction (χ) (%)[a]	Ref.
$\pi^+\pi^-$ and K^+K^-	0.02 ± 0.01	0.3	67
$\pi^+\pi^-\pi^+\pi^-$	0.16 ± 0.04	2.3	67
$\pi^+\pi^-K^+K^-$	0.14 ± 0.04	2.0	67
$\pi^+\pi^-\bar{p}p$	0.02 ± 0.01	0.3	67
$\pi^+\pi^-\pi^+\pi^-\pi^+\pi^-$	0.08 ± 0.05	1.1	67
$\gamma\psi$	1.0 ± 0.6	14	65
	2.2 ± 1.0[b]	28	68

[a] Calculated from the branching ratio products and 0.07 for the $\psi' \to \gamma\chi$ fraction. Estimates, with large uncertainties.
[b] Based on a fit to the inclusive energy spectrum of photon decay products of $\psi(3684)$.

4.4 *Properties of the Intermediate States. J, P, C, G*

It follows directly from the observation of the radiative decays $\psi' \to \gamma\chi$ that the various χ states have even charge-conjugation quantum numbers. Information needed for assignment of parity and G-parity is available only for those three intermediate states whose decays to hadrons have been observed. Each decays to one or another state of even numbers of pions and thus has even G-parity. The states $\chi(3415)$ and $\chi(3550)$ decay to $\pi^+\pi^-$ pairs and so must be of natural spin and parity 0^+, 1^-, 2^+, etc. Of these, only the even spin, even parity assignments are compatible with the even charge conjugation of the χ states.

Angular correlations (70–72) among the various particles in the cascade-decay chains $e^+e^- \to \psi' \to \gamma\chi$, $\chi \to \gamma\psi$ or $\chi \to$ hadrons depend upon the spin of the state

χ, but are uniquely determined only in the case of zero spin. For instance, photons are produced in lowest-order e^+e^- annihilation with an angular distribution of the form

$$W(\theta_{\gamma_1}) = 1 + \alpha \cos^2 \theta_{\gamma_1},$$

where θ_{γ_1} is the angle between the photon and the initial e^+ (or e^-) direction. In the case that the χ spin is zero, $\alpha = 1$. For other spins, α cannot be specified further than by the general limit $|\alpha| < 1$ without knowledge of the strengths of the various multipole contributions to the transition amplitude. Although, in contrast to the situation with nuclear transitions, there are no strong arguments justifying neglect of higher multipoles, should it happen that $E1$ amplitudes are dominant, then the magnitude of the coefficient in the angular distribution is fixed by the χ spin, i.e. $\alpha = -1/3$ for $S_\chi = 1$ and $\alpha = +1/13$ for $S_\chi = 2$.

Figures 33 and 34 show the LBL-SLAC data on angular distributions (67) of the photons produced with those χ states that have substantial branching fractions to hadronic final states. Values of the inferred anisotropy coefficients for the three χ states are $\alpha = 0.3 \pm 0.4$ for $\chi(3550)$, $\alpha = 0.1 \pm 0.4$ for $\chi(3500)$, and $\alpha = 1.4 \pm 0.4$ for $\chi(3415)$. These results indicate spin-zero for $\chi(3415)$, and at best only weakly exclude spin-zero for the other two.

For those χ states decaying to two particles, as in, for example, $\psi' \to \gamma\chi \to \gamma\pi^+\pi^-$, the distribution in angle θ' between the photon and a decay particle, in the χ rest frame, is described by a polynomial in $\cos^2 \theta'$. For the decay into two pseudoscalars, this angular correlation function is isotropic for spin-zero and contains terms in $\cos^2 \theta'$ and $\cos^4 \theta'$ for spin-two and becomes increasingly complex for higher spins. The data of the SLAC-LBL group are shown in Figure 34*a* for $\chi(3415)$ decays to pion and kaon pairs. Poor statistical accuracy precludes the

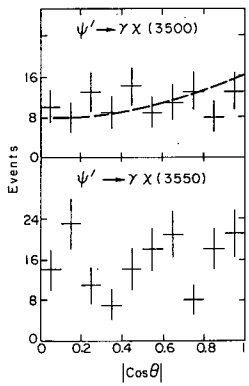

Figure 33 Distributions in the angle between the initial-state colliding beams' direction and the photons produced in $e^+e^- \to \psi(3684) \to \gamma\chi$. The χ masses are indicated in the legends. The smooth dashed curve gives the distribution for χ's of zero spin; from LBL-SLAC (67).

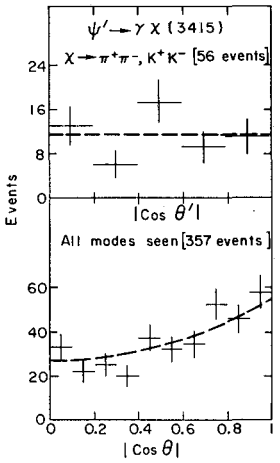

Figure 34 Angular correlations in radiative transitions $\psi(3684) \to \gamma\chi(3415)$ of psions created in e^+e^- annihilations. θ' is the angle between the photon and the dimeson direction in $\pi^+\pi^-$ or K^+K^- decays. θ is the angle between the photon and the colliding beams. The dashed curves are distributions for χ's of zero spin; from SLAC-LBL (67).

possibility of making definitive conclusions, but no deviation from isotropy is indicated, consistent with the expected distribution of the decay products of a zero-spin object.

As yet, there have been no reported measurements of angular correlations between the two photons in the cascade process $\psi' \to \gamma_1\chi \to \gamma_1\gamma_2\psi$. In this case, decays of states with angular momentum greater than zero may produce isotropic angular distributions. Lack of γ_1-γ_2 correlation is not a specific signature of zero spin. Further information about spin is contained in the correlation between γ_2 and lepton decay products of ψ in the processes $\psi' \to \gamma_1\gamma_2\psi \to \gamma_1\gamma_2 l^+ l^-$. For zero spin, that correlation function has the simple form

$$W(\theta_1, \theta_2, \phi_2, \theta_l, \phi_l) = (1 + \cos^2\theta_1)(1 + \cos^2\theta_l),$$

where θ_l and ϕ_l are the polar and azimuthal angle of a decay lepton measured from an axis defined by the γ_2 direction in the rest frame of the ψ. Expressions for decay of states with greater spin are complicated, and their forms depend again on the multipolarity of the χ transitions.

In sum, the study of decay angular distributions has yielded one conclusive result, $S_\chi = 0$ for $\chi(3415)$ and tentative suggestions that $\chi(3500)$ and $\chi(3550)$ have greater spin. Nothing is known of the spin of $\chi(3455)$, observed so far only via its $\psi\gamma$ decay mode.

4.5 *Lower-Mass States*

Searches have not uncovered odd-C states formed in e^+e^- annihilations in the energy range 1.9–3.1 GeV (see Section 5). Evidence has been presented for existence

of a state with mass near 2800 MeV/c^2, revealed in three-photon decays of $\psi(3095)$ produced in e^+e^- annihilations. Both the DASP group (50) and the Deutsches Electronen Synchrotron DESY-Heidelberg group (73, 74) measured only production angles of the three photons and determined their energies from the kinematics of the process $\psi(3095) \to 3\gamma$. The DASP data have been presented as the plot, reproduced in Figure 35, of the smallest against the largest opening angle of any pair of photons in each event. Decays of an intermediate state of unique mass in the sequence

$$\psi(3095) \to \gamma_1 X \to \gamma_1\gamma_2\gamma_3$$

produce points common to a locus determined by the mass of X. Figure 35 shows such curves for π^0, η, η' and $M_X = 2800$ MeV/c^2. An η signal is clear. A cluster of points is also shown in the region of the plot populated by events due to two-photon decays of a particle of mass $\sim$2800 MeV/c^2 produced in radiative decay of $\psi(3095)$. Calculations of background from three-photon events produced according to electrodynamics indicate smooth variation of density with mass in this region of the plot. It was concluded that a new narrow resonance had been observed with production-decay branching-ratio product

$$B[\psi \to \gamma X(2800)] \times B(X \to 2\gamma) \simeq 1.5 \times 10^{-4}.$$

Similar conclusions have been reached by the DESY-Heidelberg group, who detected three-photon events with the apparatus shown in Figure 36. The large array of NaI and lead-glass counters provides good photon-detection efficiency over $\sim$60% of the full-production solid angle. Their results are shown in Figure 37, a Dalitz plot of the lowest vs the highest γ-γ pair mass in each event. Data from

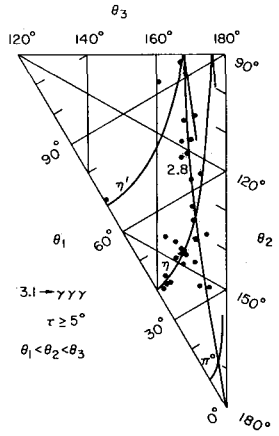

Figure 35 Scatter plot of the largest opening angle, θ_3, versus the smallest opening angle, θ_1, between any two photons in decays of $\psi(3095)$ to three photons. Loci of constant $\gamma\gamma\gamma$ invariant mass for η and η' and 2.8 GeV/c^2 are shown. Results from DASP (50) at DORIS.

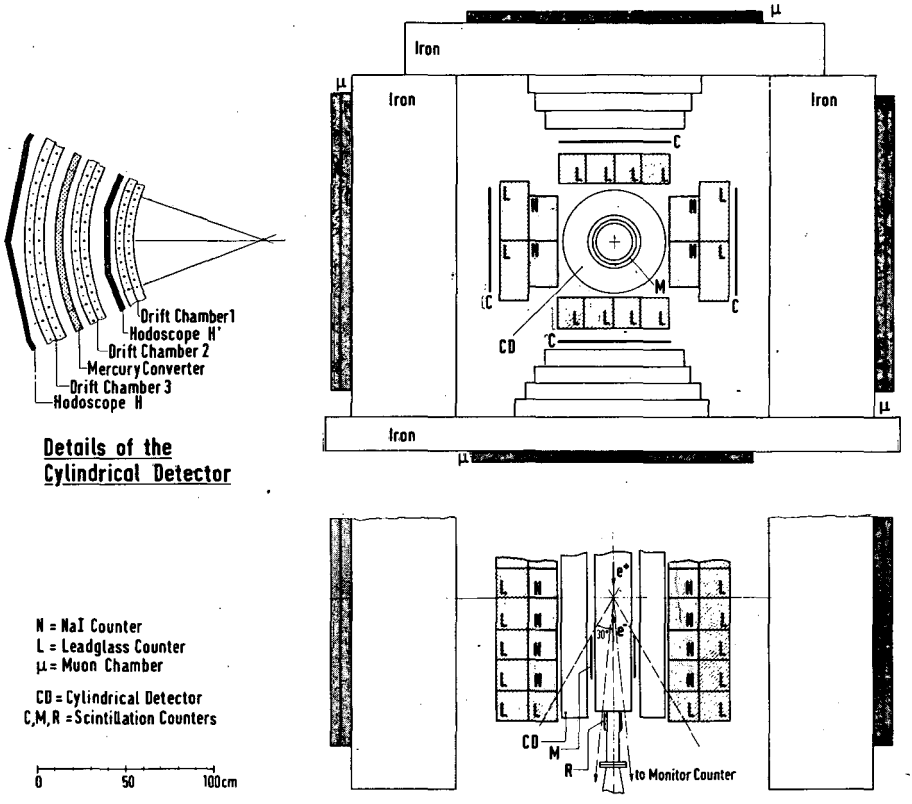

Figure 36 The DESY-Heidelberg detector apparatus at the e^+e^- intersecting storage rings DORIS (73).

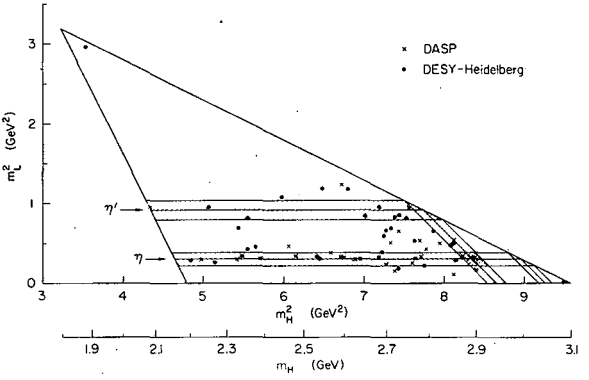

Figure 37 Dalitz plot of the smallest $\gamma\gamma$ invariant mass-squared vs the largest $\gamma\gamma$ mass-squared in $\psi(3095)$ decays to three photons. Data from DASP and DESY-Heidelberg (73).

Table 9 Properties of the intermediate states

State	Mass[a]	J^{PC}[b]	Ref.	Footnote(s)
$\chi(3415)$	3412 ± 3	0^{++}	50, 65, 67, 68	c, d
$\chi(3455)$	3454 ± 10	0^{-+}	65	e, f
$\chi(3500)$	3508 ± 4	1^{++}	50, 65, 67, 68	c
$\chi(3550)$	3553 ± 5	2^{++}	65, 67, 68	c, d

[a] Weighted averages of values quoted in the cited references.
[b] Even charge conjugation established by the radiative decay $\psi(3684) \to \psi(3095) + \gamma$.
[c] Preferred assignments of spin and parity consistent with observed angular correlations.
[d] Assignment of 0^- or 1^+ excluded by decays to $\pi^+\pi^-$ and K^+K^-.
[e] Four $\chi \to \gamma\psi$ decays observed; no evidence for hadron modes.
[f] Speculative assignment of spin and parity, neither supported nor contradicted by experimental evidence.

the DASP experiment are included. Again, the excess of events at mass near 2750 MeV/c^2 was attributed to $\gamma\gamma$ decay of a resonant state with production-decay branching-ratio product comparable to that due to η radiative production followed by $\gamma\gamma$ decay.

4.6 *Summary*

Five additional members of the ψ family have been established experimentally, albeit with reliability varying from firm [for $\chi(3415)$, $\chi(3500)$, and $\chi(3550)$] to mushy [for $X(2800)$ and $\chi(3455)$]. They are connected to the $\psi(3684)$, or $\psi(3095)$ via radiative transitions. Prodded by the suggestive level structure of a hypothesized bound quark-antiquark system, charmonium, these states have been assigned spectroscopic labels consistent with experimental results: $^3P_0$, $^3P_1$, and $^3P_2$ for the first three, and 1^1S_0 and 2^1S_0 for the others, respectively. Decays $\psi(3684) \to \chi(^3P) + \gamma$ occur with comparable branching fractions, $B(\psi' \to \gamma\chi) \simeq 0.1$, for each of the ^3P states. Properties of these states are listed in Table 9.

5 OTHER NARROW STATES, 1900 MeV/c^2 < M < 8000 MeV/c^2

A search for other narrow states coupled to lepton pairs was made by the LBL-SLAC group, which measured e^+e^--annihilation cross sections in small energy intervals from 3.2 to 7.6 GeV (75, 76). As demonstrated by the results plotted in Figure 38, none was discovered. Those results establish upper limits on the electron-pair decay widths of a resonance whose full width is much smaller than ~ 2 MeV (see Equation 3.1 with $\Gamma_h \simeq \Gamma$). Those limits are summarized in Table 10. Similar systematic searches at the storage ring ADONE, operated at energies between 1.9 and 3.1 GeV, also failed to unearth any new resonances. Limits on Γ_{ee} were established at $\sim 5\%$ of the ψe^+e^- width (77–81). Those limits are included in Table 10. Measurements at SPEAR of e^+e^--annihilation rates in coarser energy steps revealed the striking behavior near 4 GeV shown in Figure 39. At energies above the second ψ, the character of the energy dependence changes markedly.

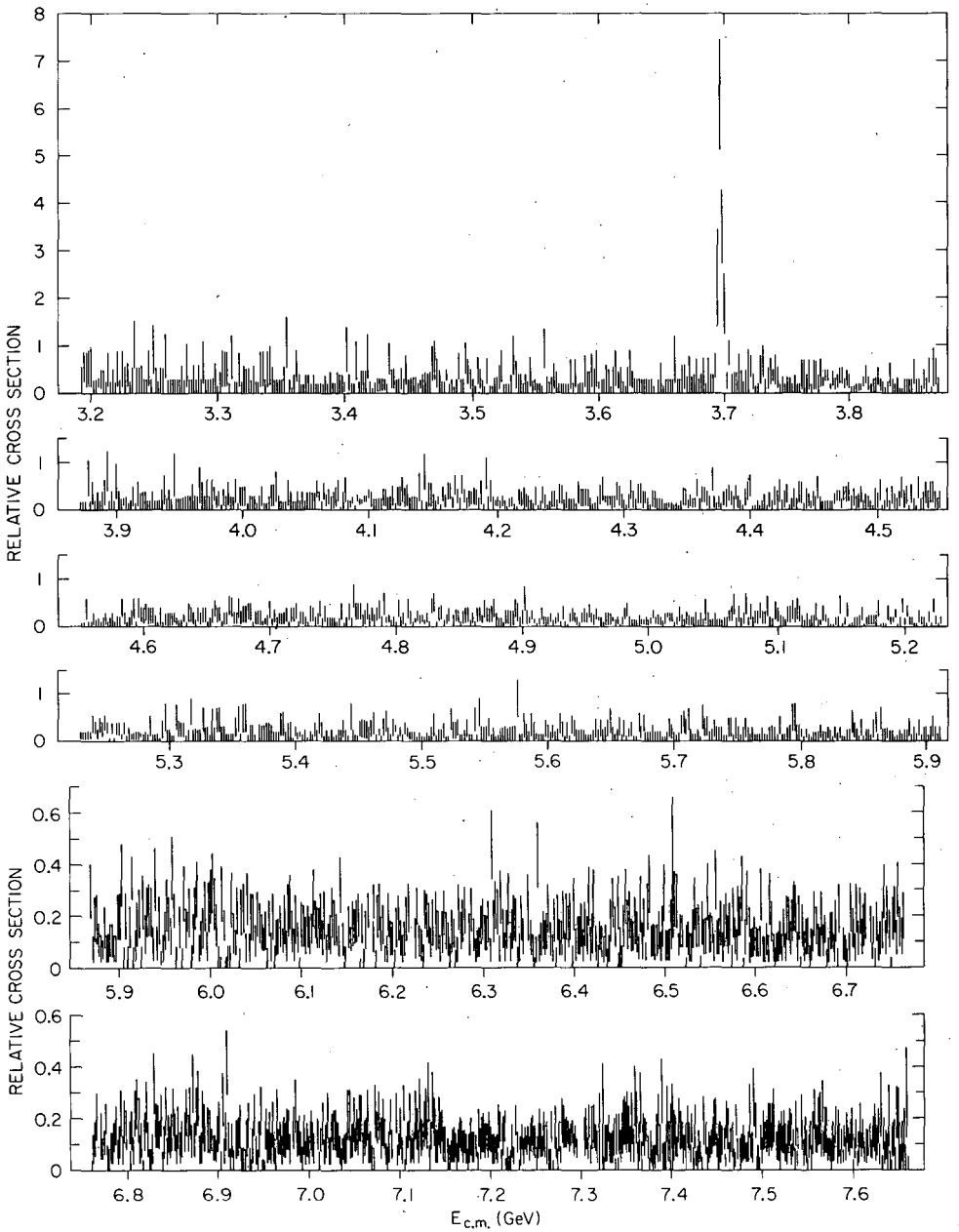

Figure 38 Energy dependence of the cross section for e^+e^- annihilation to hadrons measured at small intervals of total c.m. energy between 3.2 and 7.65 GeV; from LBL-SLAC (75, 76).

Table 10 Upper limits on parameters of narrow resonances other than $\psi(3095)$ and $\psi(3684)$

Mass range (MeV/c^2)	$\int \sigma_{Res}(E)\,dE$[a] (nb MeV)	Γ_{ee} (keV)[a]	Ref.
1910–2200	1150	0.21	77
2200–2545	800	0.20	77
2520–2595	690	0.20	81
2600–2694	1400	0.42	81
2700–2799	800	0.26	81
2800–2899	800	0.28	81
2900–3000	1600	0.62	81
2970–3090	800	0.32	78
3200–3500	970	0.47	75
3500–3680	780	0.44	75
3720–4000	850	0.55	75
4000–4400	620	0.47	75
4400–4900	580	0.54	75
4900–5400	780	0.90	76
5400–5900	800	1.11	76
5900–7600	450	0.87	76

[a] The results from ADONE (77, 78, 81) have been presented as ratios of upper limits on the integrated resonance cross section to the $\psi(3095)$ integrated cross section measured with the same apparatus. To eliminate effects of different detection efficiencies, we have used the SLAC-LBL value of the $\psi(3095)$ lepton-pair partial width (Table 3) in calculating the limits on the integrals and Γ_{ee} listed here (see Equation 3.4).

Below 4 GeV, the ratio of nonresonant hadronic to muon-pair cross sections, R, is essentially constant at $\simeq 2.5$. Above 4 GeV, R is also constant, but larger: $R \simeq 5.5$. In the transition interval, there appears to be a series of resonant structures that, however many there are, have widths more comparable to those of the lighter vector mesons than the ψ particles at 3095 and 3684 MeV/c^2.

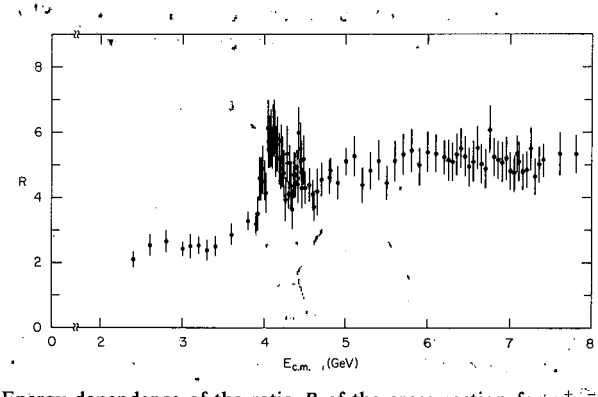

Figure 39 Energy dependence of the ratio R of the cross section for e^+e^- annihilation to hadrons to that for annihilation to muon pairs; from SLAC-LBL (76).

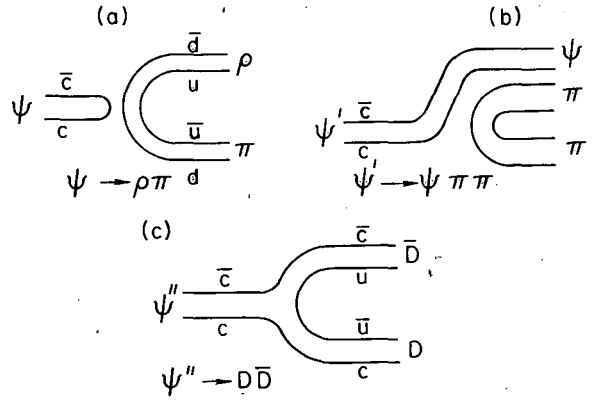

Figure 41 Duality diagrams of OZI-forbidden psion decays to (*a*) ordinary hadrons and (*b*) $\psi\pi\pi$; (*c*) OZI-allowed decays to charmed-meson pairs.

The empirical OZI rule must be invoked to provide a means of inhibiting the decays of the $c\bar{c}$ states to ordinary mesons composed only of *u*, *d*, or *s* quark-antiquark pairs. Strong, charm-conserving decays can proceed only to states containing *D* mesons, as depicted in the duality diagrams of Figure 41. Kinematics is invoked to prohibit decay to charmed mesons, whose masses must then be greater than 1842 MeV/c^2. Calculations have been made by De Rujula et al (91) of hadron masses in a general theory of quark confinement. Their estimates of the

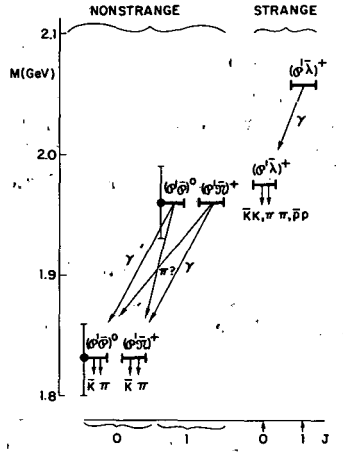

Figure 42 Spectrum of masses of lowest-lying charmed mesons as predicted by De Rujula, Georgi & Glashow (91). Their notation for the quark constituents may be readily translated to *u*, *d*, *s*, and *c*.

masses of charmed S-state quark-antiquark bound systems are shown as the energy level diagram of Figure 42. The results, admittedly not very precise, support the experimental requirement that $\psi(3684)$ be still below threshold for decay to charmed mesons. It should be noted, in this connection, that the energy dependence of the e^+e^--annihilation cross section (see Figure 39) behaves very much as if there were a threshold for pair production of particles of mass between 1.85 and 2.0 GeV/c^2. Also, the photoproduction results of Figure 13 invite a speculative interpretation in terms of a threshold at ~ 5 GeV energy for the inelastic, charm-conserving, OZI-allowed reaction $\psi N \to D\bar{D}N$, producing a pair of charmed mesons.

Identification of the psions with $c\bar{c}$ bound states requires comparison with the complete spectrum of such states. Even before the first ψ discovery, Appelquist & Politzer (5), reasoning from ideas of asymptotic freedom, expounded the view that this system of bound massive quarks could be described as a nonrelativistic atomic system, charmonium, that is analogous to positronium. Properties of charmonium states are determined by the combined effects of short-range $c\bar{c}$ interactions via exchange of massless vector gluons and some long-range confining potential. The pattern of charmonium energy levels that emerges, labeled with spectroscopic notation, is shown schematically in Figure 43. The pattern of observed energy levels is plotted suggestively in Figure 44, with $\psi(3095)$ the lowest-lying $^3S_1$ state and $\psi(3684)$ the first radially excited $^3S_1$ state. Remarkable qualitative agreement with the model predictions is apparent. That statement must be tempered with the reminder that the identities of the intermediate states have not been firmly established. Spins and parities of the intermediate χ states have been tentatively assigned values consistent with experimental data. Some theoretical arguments of Chanowitz & Gilman (92), based on quantitative predictions of radiative decay widths, have been brought to bear in assigning $\chi(3510)$, rather than $\chi(3445)$, the $^3P_1$ classification.

Numerous more or less quantitative predictions of level spacings, hadronic decay rates, leptonic decay rates, and radiative transition rates are available for comparison with the data. We briefly consider a selection from among the results of those calculations.

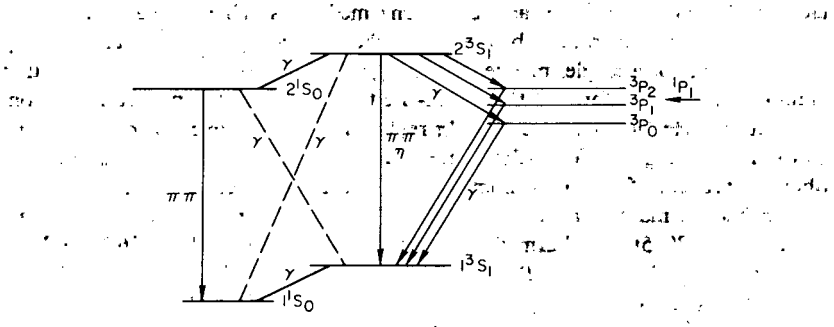

Figure 43 Schematic diagram of the energy levels of charmonium, the bound system of a charmed quark and its antiparticle. Some transition modes are indicated. See Appelquist & Politzer (5), for example.

Table 12 Selection rules for weak decays of charmed particles

Decay-amplitude θ_c dependence	Selection rules	Examples
$\cos\theta_c$	$\Delta S = \Delta C = \Delta Q = \pm 1, \lvert\Delta I\rvert = 0$	$D^0 \to K^-\mu^+\nu$ $F^+ \to \mu^+\nu$ $\Lambda_c^+ \to \Lambda^0 e^+\nu$
$\sin\theta_c$	$\Delta S = 0, \Delta C = \Delta Q = \pm 1, \lvert\Delta I\rvert = \frac{1}{2}$	$D^+ \to \mu^+\nu$ $F^+ \to K^0\mu^+\nu$ $\Sigma_c^{2+} \to pe^+\nu$
$\cos^2\theta_c$	$\Delta S = \Delta C = \pm 1, \lvert\Delta I\rvert = 1$	$D^0 \to K^-\pi^+$ $D^\pm \to K^\mp\pi^\pm\pi^\pm$ $F^+ \to K^+K^-\pi^+$ $\Lambda_c^+ \to \Lambda^0\pi^+\pi^+\pi^-$
$\cos\theta_c \sin\theta_c$	$\Delta S = 0, \Delta C = \pm 1, \lvert\Delta I\rvert = \frac{1}{2}, \frac{3}{2}$	$D^0 \to \pi^+\pi^-$ $F^+ \to K^0\pi^+$ $\Lambda_c^+ \to n\pi^+$
$\sin^2\theta_c$	$\Delta S = -\Delta C = \pm 1, \lvert\Delta I\rvert = 0, 1$	$D^0 \to K^+\pi^-$ $D^\pm \to K^\pm\pi^-\pi^+$ $F^+ \to K^+K^+\pi^-$ $\Xi_c^0 \to p\pi^-$

is charm- as well as strangeness-conserving. Decay selection rules, or rather, ordering of amplitude strengths, are implicit in the form of the charged hadronic current

$$J_{h_\nu} = \bar{u}\gamma_\nu(1+\gamma_5)[d\cos\theta_c + s\sin\theta_c] + \bar{c}\gamma_\nu(1+\gamma_5)[-d\sin\theta_c + s\cos\theta_c],$$

where θ_c is the Cabibbo rotation angle ($\simeq 0.23$ radians). Decays involving quark-constituent transformations $c \to s$ are favored because of the presence of $\cos\theta_c$ in their transition amplitudes. We list in Table 12 selection rules corresponding to the θ_c dependence of the decay amplitudes and some selected examples of charmed-particle decay modes that obey those rules. Meson decay rates have been estimated to be $\sim 10^9$ sec^{-1} for leptonic, $\sim 10^{12}$ for semileptonic, and $\sim 10^{13}$ sec^{-1} for hadronic modes (90). There do not exist reliable estimates for partial widths for decays to the various allowed final states of hadrons, although naive phase-space considerations lead to the expectation of relatively low average multiplicity. Such simple-minded arguments may require significant modification on consideration of the role of resonant states as decay products.

7. STATES HEAVIER THAN 4000 MeV/c^2

The LBL-SLAC group has reported results of detailed measurements of the e^+e^--annihilation cross section in the energy interval 3.9–4.6 GeV (101). Detection efficiency determined from a Monte Carlo simulation of the apparatus' response varied from 0.53 at the lowest energy to 0.57 at the highest. Possible systematic errors in absolute scale are estimated to be $\sim \pm 15\%$, the result of uncertainties in the efficiency calculation. Those errors should introduce smaller relative varia-

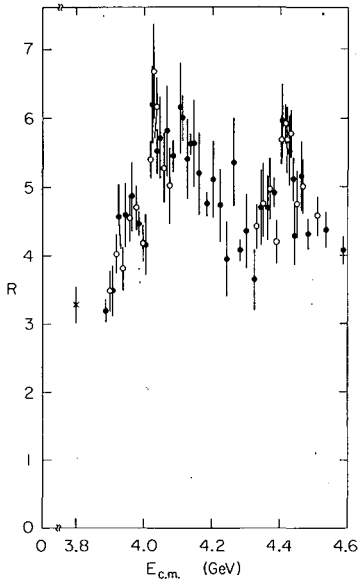

Figure 46 Energy dependence of the ratio $R = \sigma(e^+e^- \rightarrow \text{hadrons})/\sigma(e^+e^- \rightarrow \mu^+\mu^-)$ at c.m. energies between 3.8 and 4.6 GeV; from LBL-SLAC (101).

tions, less than 5%, among the values at the various energies. Figure 46 shows the data, plotted again as the ratio of hadronic-annihilation cross section to the muon-pair cross section, with statistical errors indicated. At the very least, two peaks are evident. It is, however, not possible to determine details of the structure in the variation of R with energy between 3.9 and 4.3 GeV. There appear to be a number of resonances; there may be thresholds for production of new particles. Interferences among resonant amplitudes may also account for some of the violent appearance of this substructure.

The data in the interval $\sim$4.3–$\sim$4.6 GeV appear more consistent with the presence of a single, isolated resonant state, as seen in Figure 47. A fit was made

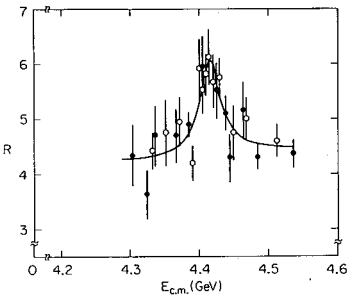

Figure 47 Resonance fit to the energy dependence of R near 4.4 GeV. See text for parameters of the state; from SLAC-LBL (101).

to a Breit-Wigner line shape, including radiative corrections, with a noninterfering background. Resonance parameters determined from the fit are shown in Table 3, together with those for $\psi(3095)$ and $\psi(3684)$, for comparison. The striking feature of this resonance is the magnitude of its full width, $\Gamma(4414) = 33 \pm 10$ MeV, more characteristic of strong decay than of the inhibited decay of $\psi(3095)$ and $\psi(3684)$. The electron width $\Gamma_{ee} = 0.44 \pm 0.14$ keV is one fifth that of $\psi(3684)$. Branching ratios to particular distinct hadronic final states have not as yet been determined.

A resonance at $\sim$4.4 GeV is nicely qualitatively compatible with an interpretation as an anticipated higher excitation of the charmonium structure. Indeed, as discussed above, two $^3S_1$ states may be expected in the energy interval 3.9–4.5 GeV. The smaller lepton-pair partial width of $\psi(4414)$ needs to be accounted for with a decreased modulus-squared of the wave function at zero separation, $|\psi(0)|^2$, of the higher-energy bound eigenstate. Unfortunately, all $^3S_1$ $c\bar{c}$ eigenfunctions have the same value of $|\psi(0)|^2$, independent of principal quantum number, in the simplest model of a long-range binding potential, linearly rising with distance. Some "tuning" of the shape of the potential is required if the charmonium model is to give more than a qualitative description of the psionic states.

Two orders of magnitude increase in total width, compared to $\psi(3684)$, indicate that the OZI suppression mechanism has ceased to operate on $\psi(4414)$ decays. If the hidden charm interpretation of psions is to be maintained, it must be that this resonance rest energy is above the threshold for decay to pairs of particles bearing exposed charm.

8 CHARMED PARTICLES

Following some years of unsuccessful searches for charmed particles produced in hadron-hadron collisions (102) and in e^+e^- annihilations (103), all but conclusive evidence for their existence has been obtained by the LBL-SLAC group (104, 105), who observed decays of charmed mesons produced in e^+e^- annihilations, and by Knapp et al (106), who detected decays of photoproduced charmed baryons.

8.1 *Mesons*

In the LBL-SLAC experiment, evidence for $K\pi$ and $K\pi\pi\pi$ decay modes of charmed mesons was found in a study of 29,000 multiprong events produced in e^+e^- annihilations at c.m. energy between 3.90 and 4.60 GeV. The data are summarized succinctly in the effective-mass plots of Figure 48. A significant signal is evident near 1900 MeV/c^2 in the effective-mass distributions of all neutral combinations of two charged particles to which kaon mass and pion mass were arbitrarily assigned. Independent measurements of momentum and time of flight are made with the detection apparatus, but the timing resolution, 0.4 nsec, is insufficient to allow a distinction to be made between pions and kaons whose flight times in these events typically differ by 0.5 nsec. To make use of the time-of-flight information, the alternate mass assignments to each track were assigned relative weights appropriate to a Gaussian probability distribution with $\sigma = 0.4$ nsec:

$$W_i = \exp\left[-(t_i - t_T)^2/2\sigma^2\right],$$

where t_i is the flight time for mass m_i, determined from measured track parameters, and t_T is the directly measured time. The sum of track weights is made equal to unity and each mass combination, $\pi\pi$, πK, and KK, assigned a weight equal to the product of the track weights. With this method, the sum of weights assigned to all mass combinations just equals the total number of two-particle combinations in each event, so that there is no double counting. The second row of Figure 48 shows the invariant-mass spectra. A clear peak is evident in the $K^{\pm}\pi^{\mp}$ mass distribution, and the small residual signals in $\pi\pi$ and KK are understood to result from misidentification of true $K^{\pm}\pi^{\mp}$ events expected from inaccurate time-of-flight measurements. In the third row of Figure 48 are similarly weighted distributions, showing a peak in $K\pi\pi\pi$ at essentially the same mass as the $K\pi$ combinations. No significant signals were found in corresponding doubly charged two- or four-particle mass spectra.

Fits to the data with assumed Gaussian-shaped peaks above smoothly varying backgrounds yielded central values of mass 1870 and 1860 MeV/c^2 for $K\pi$ and $K\pi\pi\pi$, respectively. With consideration of the effects of systematic and random errors, it was concluded that both mass distributions are consistent with having a common source, decays of a particle of mass $M(D^0) = 1865 \pm 15$ MeV/c^2. The

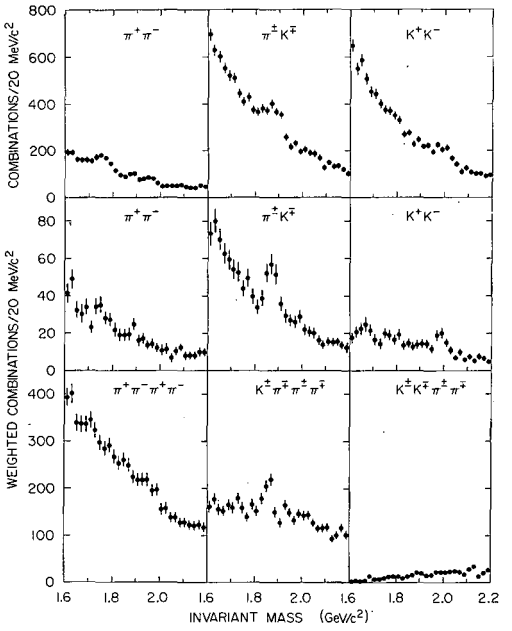

Figure 48 Inclusive neutral two- and four-particle invariant-mass spectra in multihadronic e^+e^- annihilation at c.m. energies 3.9–4.6 GeV. Top row, indiscriminate-mass assignments; middle row, mass assignments with time-of-flight weighting; bottom row, four-body mass assignments with time-of-flight weighting; from LBL-SLAC (104).

observed widths of the mass peaks are those expected from experimental resolution alone, 25 MeV/c^2 (rms) for the $K\pi$ system and 13 MeV/c^2 for the $K3\pi$ system, but a finite width of the state was not definitively excluded. A 90% confidence limit of 40 MeV/c^2 was deduced for the resonance decay width, based on quality of fits of a Breit-Wigner resonance shape convoluted with a Gaussian resolution function.

Peruzzi et al (105) report similar observations of peaks in effective-mass distribution of $K^-\pi^+\pi^+$ and $K^+\pi^-\pi^-$ combinations selected from multihadron e^+e^- annihilations at a c.m. energy of 4.03 GeV/c. Those data were obtained in a run at SPEAR with the LBL-SLAC magnetic detector, stimulated by the observation of the D^0 decays. Invariant mass spectra are shown in Figure 49 for three-body mass combinations, with $K\pi\pi$ mass assigned and each event weighted according to the prescription discussed above. Events with $\pi^+\pi^-$ pairs in the final state show no evidence of resonance peaks in their mass distributions, while a clear peak appears, at $M(D^{\pm}) = 1876 \pm 15$ MeV/c^2, in the exotic $K^-\pi^+\pi^+$ and $K^+\pi^-\pi^-$ states. That peak again has the appearance of resulting from decays of a resonance state whose width is a creature of merely experimental resolution. As with the neutral state, the 90% confidence-level upper limit to the width of the resonance is 40 MeV/c^2. Charged and neutral masses are equal within errors, but the measurements allow of a mass splitting of some 10 MeV/c^2, not atypical of splittings within isospin multiplets. It is natural and sensible then to identify the charged $K^{\pm}\pi^{\mp}\pi^{\mp}$ events as members of an isospin multiplet whose neutral partners are the D^0 mesons whose decays were revealed in $K^{\pm}\pi^{\mp}$ and $K^{\pm}\pi^{\mp}\pi^+\pi^-$ modes.

Charmed mesons must be produced in particle-antiparticle pairs in the annihilation of uncharmed positrons on electrons. Two pieces of experimental evidence

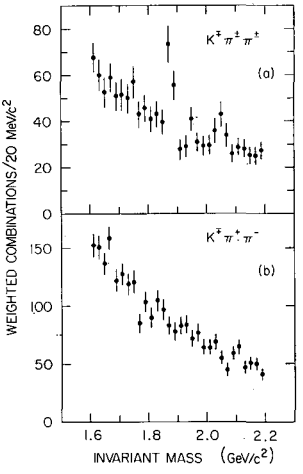

Figure 49 Inclusive mass spectra of charged three-particle combinations in multihadron products of e^+e^- annihilations at 4.03-GeV c.m. energy. Mass assigned according to time-of-flight weights in (*a*) exotic and (*b*) nonexotic systems; from SLAC-LBL (105).

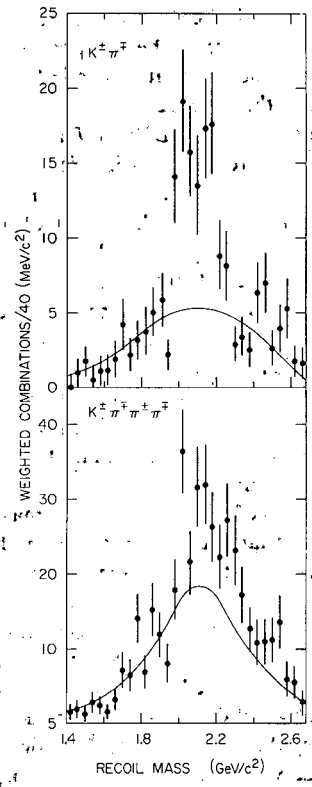

Figure 50 Distribution of masses accompanying $K^{\pm}\pi^{\mp}$ and $K^{\pm}\pi^{\mp}\pi^{+}\pi^{-}$ in events with $K\pi$, $K3\pi$-invariant masses in the peaks near 1865 MeV/c^2 seen in Figure 48. The smooth curves show background shapes obtained from events with $K\pi$ and $K3\pi$ masses adjacent to the peaks; from LBL-SLAC (104).

have been brought to bear on the question of the process by which the D^0 and $D^{\pm}$ mesons are produced. First, the observed spectra of masses recoiling against the $(K\pi)^0$, $(K3\pi)^0$, and $(K\pi\pi)^{\pm}$ systems with masses in the resonance region give evidence that the D mesons are produced in association with systems whose masses are greater than $\sim$1870 MeV/c^2. Figures 50 and 51 show those recoil-mass spectra for the D^0 and $D^{\pm}$ peaks, respectively, both with estimated background indicated. All three spectra show evidence of a recoil system with well-defined mass near 2000 MeV/c^2. A second peak near 2200 MeV/c^2 appears in the spectra of masses accompanying the neutral $K\pi$ and $K3\pi$ combinations. Since there is little signal above background near 1870 MeV/c^2 in any of the recoil-mass distributions, $\bar{D}D$-associated production must be a minor contributing process. Although the data are hardly conclusive, the results suggest that some D^0's and $D^{\pm}$ whose decays are observed are produced in the cascade decay of a heavier, narrow-width object.

with the recognition of parity violation in the weak interaction. A sample of $K\pi\pi$ decays of $D^{\pm}$ was chosen from events produced in $e^{\pm}$ annihilations at c.m. energy between 3.9 and 4.25 GeV, restricted to those $K\pi\pi$ combinations accompanied by missing mass between 1.96 and 2.04 GeV, a procedure that produced 70 events in a narrow peak above a background of some 50 events. A Dalitz plot for those $K\pi\pi$ combinations with mass between 1860 and 1920 MeV/c^2 has density indistinguishable from uniform. Figure 52 shows the data divided into Dalitz-plot regions chosen to be equally populated by decays of 0^- mesons, but populated in the ratio $\sim 1/8$ for spin-parity 1^- and $\sim 1/6$ for spin-parity 2^+ meson decays. In both cases, the observed population ratio is unity to within errors; $J^P = 1^-$ is excluded to a confidence level 2×10^{-5}, 2^+ is ruled out with a confidence level of 0.002. Since three pseudoscalars cannot be in a zero-spin, even-parity state, only 0^- is a possible $D^{\pm}$ spin-parity assignment, unless the spin is more than two. However, the $K\pi$ state has natural spin parity. Presuming $D^{\pm}$ and D^0 to be members of an isospin multiplet and so to have the same parity, the observations show that the decay proceeds with comparable rates to states of opposite parity, and it follows that the decay interaction is parity-violating, another property of charmed mesons.

Presented with this assemblage of properties congruent to those of the predicted particles, it makes sense to end the reticence maintained by the experimentalists and recognize the discovery of charmed mesons.

8.2 *Baryons*

One other member of the charmed-particle family has been established with reasonable certainty, a charmed baryon. Knapp et al (106) have reported observation of a sharp peak in the mass spectrum of $\bar{\Lambda}\pi^+\pi^-\pi^-$ produced by photons interacting with beryllium. Some details of the experimental arrangement have been presented above in the discussion of ψ production by this group at Fermilab. Identification of Λ^0 and $\bar{\Lambda}^0$ decays is beyond question, as shown in the mass plots of Figure 53. Evidence of a negatively-charged narrow state decaying to $\bar{\Lambda}\pi^+\pi^-\pi^-$ is shown in the invariant-mass plots of Figure 54. Also shown there is the nonexistence of a positively charged partner, $\bar{\Lambda}\pi^+\pi^+\pi^-$. The state's mass was determined to be 2260 ± 10 MeV/c^2 and the measured full width of the peak is (40 ± 20) MeV/c^2. That width is consistent with the estimated experimental mass resolution of a zero-width state. Some evidence was found for a cascade decay of a heavier particle of mass ~ 2500 MeV/c^2 to the $\Lambda(3\pi)^-$ and a positive pion, as shown in Figure 55. There is a clear peak in the distribution of the difference in mass between the $\bar{\Lambda}(4\pi)^0$ combinations and those $\Lambda(3\pi)^-$ combinations with mass near the 2260 peak value. Those data indicate a cascade process

$$\bar{\Lambda}\pi^-\pi^-\pi^+\pi^+(\sim 2.5\ \text{GeV}/c^2) \rightarrow \bar{\Lambda}\pi^-\pi^-\pi^+(2.26\ \text{GeV}/c^2) + \pi^+.$$

A charmed antibaryon with charge -1 has quark components $\bar{c}\bar{u}\bar{d}$, i.e. one charmed antiquark and two uncharmed antiquarks. It is impossible to construct a charmed, positively charged antibaryon with a charmed antiquark and two ordinary antiquarks. It is natural to identify and classify the particle decaying to the

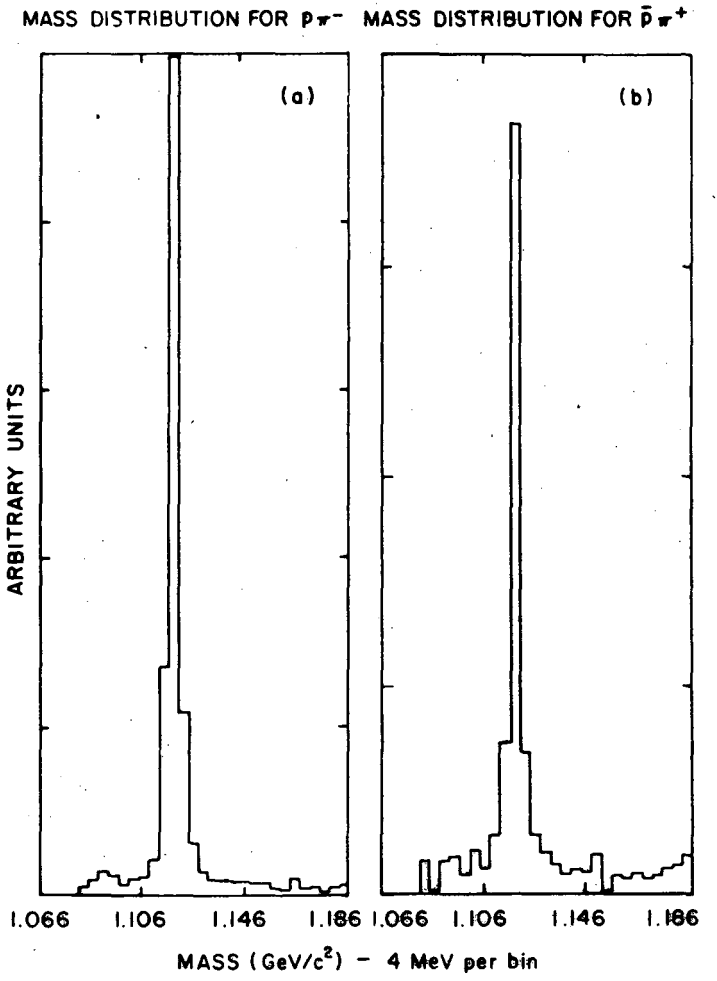

Figure 53 Invariant mass distributions of (*a*) $p\pi^-$ and (*b*) $\bar{p}\pi^+$ V^0's in multihadron states photoproduced at ~250 GeV; from Knapp et al (106) at Fermilab.

$\bar{\Lambda}\pi^+\pi^-\pi^-$ system at 2260 MeV/c^2 as the charmed antibaryon $\bar{\Lambda}_c(\bar{c}\bar{u}\bar{d})$. Its higher-mass parent is then recognized as either $\bar{\Sigma}_c^0(\bar{c}\bar{d}\bar{d})$, a spin-$\frac{1}{2}$, $I = 1$ charmed baryon or $\bar{\Sigma}_c^{*0}(\bar{c}\bar{d}\bar{d})$ of spin $\frac{3}{2}$, isospin 1.

A single example of just such a production-decay sequence had previously been found among events initiated by neutrino interactions in a hydrogen bubble chamber (108). The event, shown in Figure 56, is interpreted as an example of the reaction $\nu p \to \mu^- \Lambda^0 \pi^+ \pi^+ \pi^+ \pi^-$. With those assignments of particle identities, the mass of the $(\Lambda 4\pi)^{2+}$ system is calculated to be 2426 ± 12 MeV/c^2 and the three possible

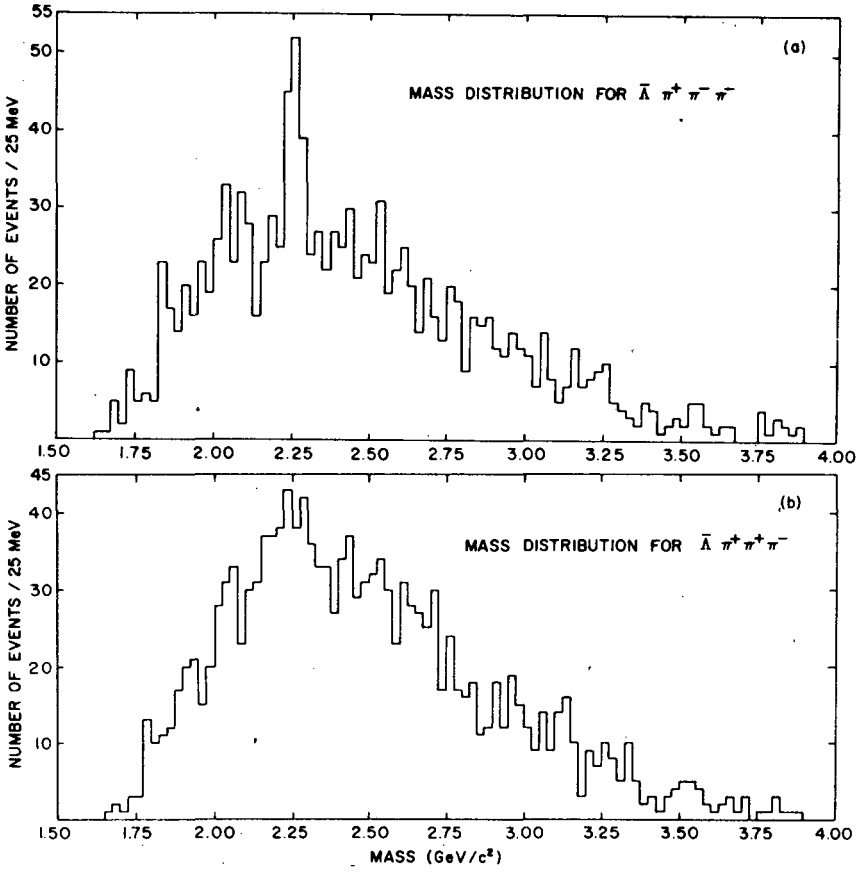

Figure 54 Distribution of invariant masses for (*a*) $\bar{\Lambda}(3\pi)^-$ and (*b*) $\bar{\Lambda}(3\pi)^+$ combinations in multihadron states photoproduced at ~250 GeV; from Knapp et al (106).

$(\Lambda\pi^+\pi^+\pi^-)$ combinations are found to be smaller in mass by 166 ± 15 MeV/c^2, 338 ± 12 MeV/c^2, and 327 ± 12 MeV/c^2. Noting that this reaction violates the selection rule $\Delta S = \Delta Q$ for ordinary hadrons, it was suggested that this event is an example of the sequential reactions, beginning with weak production of a charmed baryon

$$\nu p \to \Sigma_c^{2+}(cuu)\mu^- \left[\text{or } \Sigma_c^{*2+}(cuu)\mu^-\right],$$

Figure 55 Evidence for the cascade process $\bar{\Lambda}(4\pi)^0 \to \bar{\Lambda}(3\pi)^-\pi^+$ in multihadron states photoproduced at 250 GeV. (*a*) $\bar{\Lambda}(4\pi)^0$ invariant-mass spectrum; (*b*) $\bar{\Lambda}(3\pi)^-$ invariant-mass spectrum; (*c*) difference in mass between $\bar{\Lambda}(4\pi)^0$ and $\bar{\Lambda}(3\pi)^-$ combinations shown as the solid histogram for $\bar{\Lambda}(3\pi)^-$ masses in the peak at ~2.25 GeV/c^2 and as the dashed histogram for $\bar{\Lambda}(3\pi)^-$ just outside the peak; from Knapp et al (106).

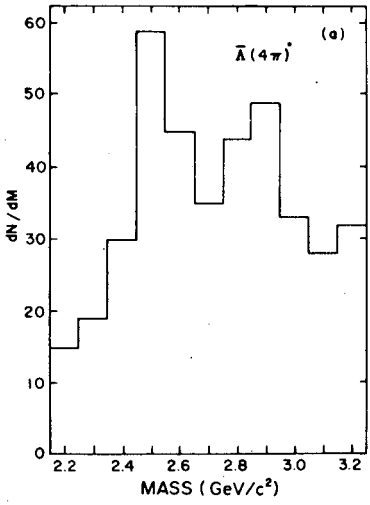
(a)
$\bar{\Lambda}(4\pi)^+$
dN/dM
MASS (GeV/c²)

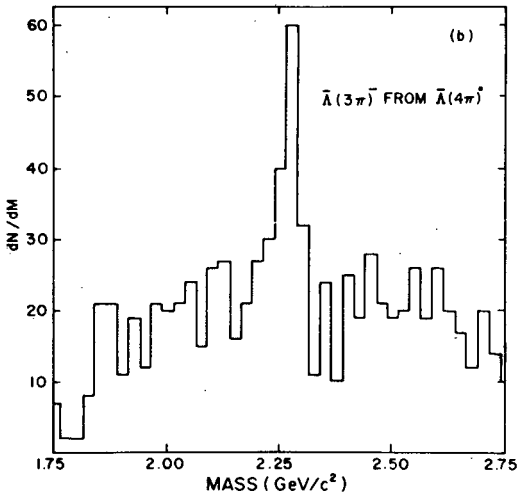
(b)
$\bar{\Lambda}(3\pi)^-$ FROM $\bar{\Lambda}(4\pi)^+$
dN/dM
MASS (GeV/c²)

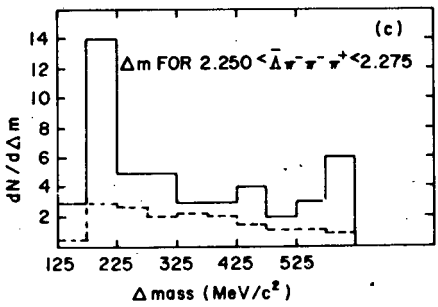
(c)
Δm FOR 2.250 < $\bar{\Lambda}\pi^-\pi^-\pi^+$ < 2.275
dN/dΔm
Δ mass (MeV/c²)

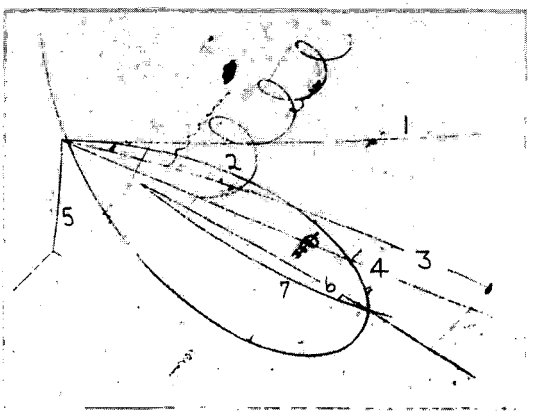

Figure 56 View of an event interpreted as an example of $\nu p \to \mu^- \Lambda^0 \pi^+ \pi^+ \pi^+ \pi^-$ produced in the BNL liquid-hydrogen bubble chamber. The Λ^0 is particularly conspicuous as tracks 6 and 7; observation of Cazzoli et al (108) at Brookhaven National Laboratory.

followed by strong decay

$$\Sigma_c^{2+} \text{ (or } \Sigma_c^{*2+}) \to \Lambda_c^+ (cud)\pi^+,$$

and the succeeding, favored weak decay

$$\Lambda_c^+ \to \Lambda^0 \pi^+ \pi^+ \pi^-.$$

The notation here is the same as above, indicating quark contents and spins. Particularly noteworthy are the remarkable coincidences between the masses of these objects and those predicted by De Rujula et al (91), i.e. 2250 MeV/c^2 for Λ_c, 2410 MeV/c^2 for Σ_c, and 2480 MeV/c^2 for Σ_c^*.

8.3 *Miscellany*

Other observations have provided more indirect evidence of the presence of charmed-quark components of hadrons. Events with two muons produced in high-energy neutrino-nucleon interactions have been interpreted in terms of production of new particles and their subsequent weak leptonic or semileptonic decays (109, 110). From the measured characteristics of the events, Benvenuti et al (109) deduce that the new particle, if a hadron, has mass between ~ 2 and ~ 4 GeV/c^2 and has a lifetime less than 10^{-10} sec.

Events with a negative muon, positron, and neutral strange particle in the final state have been observed as products of neutrino-initiated reactions in bubble chambers. Von Krogh et al (111) found four examples of the reaction $\nu_\mu N \to \mu^- e^+ K_s^0 X$ in an exposure of the Fermi National Accelerator Laboratory FNAL 15-ft bubble chamber filled with a neon-hydrogen mixture. Blietschau et al (112) have reported observation of three examples of $\nu_\mu N \to \mu^- e^+ V^0 (K^0 \text{ or } \Lambda^0) X$ in the freon-filled bubble chamber Gargamelle exposed to a neutrino beam at CERN.

One may surmise (both groups have) that these events show cascade production and semileptonic decay of charmed hadrons of mass about 2000 MeV/c^2.

Semileptonic decays of charmed hadrons have been invoked to explain the single-electron-plus-hadrons final states made in e^+e^- annihilations at c.m. energies between 4.0 and 4.2 GeV and detected in the DASP apparatus (113). For improved electron detection in this experiment, the apparatus of Figure 15 was supplemented with threshold Cerenkov counters on each side of the intersection region at DORIS. Of 87 electron + hadron events, 28 survived cuts on shower-counter pulse height, electron momentum, and vertex position. Of these, 22 had hadron multiplicity of four or greater. Calculated rates for conventional sources of these events are too low to account for any but a small fraction of those detected. In data taken at c.m. energies less than 3.7 GeV, events of this type did not occur with greater than calculated background rates. The electron-momentum distribution reproduced in Figure 57 disagrees with that expected of electron-decay products of a heavy lepton of mass 1.9 GeV/c^2, a conceivable source of the events. The posited new hadrons whose semileptonic decays are presumed to have been observed are to have mass between 1.8 and 2.1 GeV/c^2 and to be supplied with a new quantum number (charm, perhaps) conserved in strong and electromagnetic processes.

Rates for e^+e^- annihilations to states with a neutral K meson and an electron have been measured as a function of c.m. energy by Burmester et al (114) with the magnetic detector PLUTO at DORIS. That apparatus consists of fourteen cylin-

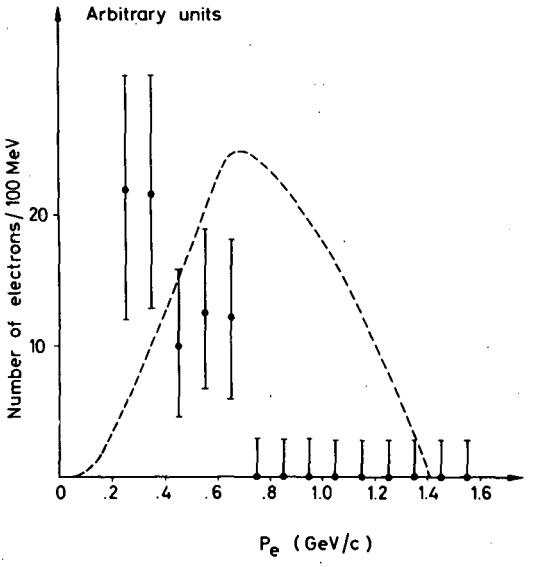

Figure 57 Inclusive momentum distribution of electrons in multiparticle e^+e^- annihilations at energies of 4.0–4.2 GeV. Events with multiplicity of four or greater are included. The dashed smooth curve shows a calculated distribution of electrons from decay of a 1.9-GeV/c^2 heavy lepton; from DASP (113).

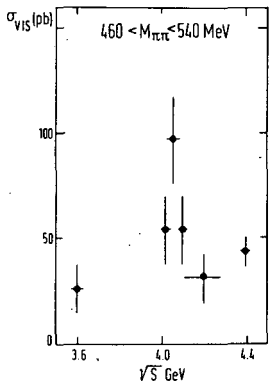

Figure 58 Energy dependence of the yield of detected correlated $K_S^0 e^{\pm}$ combinations in multiparticle states made in e^+e^- annihilations; from PLUTO (114) at DORIS.

drical proportional wire chambers arrayed coaxially about the direction of the intersecting beams. Two cylindrical lead converters, 0.44 and 1.7 radiation lengths thick, with following wire chambers provide for detection of electron-initiated electromagnetic showers. A super conducting coil surrounding the track-sampling chambers produces a 20,000-G magnetic field directed parallel to the axis of the detector array. Clear evidence for K^0 production was found in distributions of invariant mass of oppositely charged tracks in multiparticle events. Figure 58 shows the observed energy dependence of the detected yield of $e^{\pm}K_s^0(\rightarrow \pi^+\pi^-)$ events, the K_s^0's having been chosen as $\pi^+\pi^-$ pairs with mass in the observed peaks between 460 and 540 MeV/c^2. After background subtraction and correction for deficiencies, Burmester et al arrive at an estimated inclusive cross section at the maximum, $\sigma(e^+e^- \rightarrow e^{\pm}K^0 + \text{anything}) \simeq 3$ nb, accurate to about a factor of 2.

Table 13 Properties of observed narrow states with classifications as charmed hadrons

State	Mass (MeV/c^2)	Decay modes	Ref.	Footnote(s)
$D^0, \bar{D}^0$	1865 ± 15	$K^{\pm}\pi^{\mp}, K^{\pm}\pi^{\mp}\pi^+\pi^-$	104	a
$D^{\pm}$	1876 ± 15	$K^{\pm}\pi^{\mp}\pi^{\mp}$	105	a
$\bar{\Lambda}_c^-$	2260 ± 10	$\bar{\Lambda}\pi^-\pi^-\pi^+$	106	—
Λ_c^+	2260 ± 15	$\Lambda\pi^+\pi^+\pi^-$	108	b, c
$\bar{\Sigma}_c^0$	~ 2500	$\bar{\Lambda}_c^-\pi^+$	106	d
Σ_c^{2+}	2426 ± 12	$\Lambda_c^+\pi^+$	108	b, d

[a] Presuming these to be isospin partners, parity violation in their decays has been demonstrated (107).
[b] One event with a cascade decay.
[c] Mass not uniquely determined. One of three possible $\Lambda\pi^+\pi^+\pi^-$ from decay of the Σ_c^{2+} (see text for others).
[d] Not uniquely classified. May be excited state Σ_c^*.

These data are proffered as evidence for the presence of charmed mesons whose semileptonic decays, $D^{\pm} \to K^0 e^{\pm} \nu$ have been detected. Boldly accepting that interpretation, and presuming ~ 10 nb (of the 30 nb total) to be the cross section for production of charged D-meson pairs in e^+e^- annihilations at 4.05 GeV, we may make the rough estimate $\sim(3/2)/10 = 15\%$, for the *Kev* decay branching ratio. That value is not incompatible with crude theoretical estimates (90) of charmed-meson decay rates.

8.4 *Summary*

New mesons and baryons of long lifetime have been observed. Their currently established masses, modes of production, and decay characteristics, as listed in Table 13, correspond without exception to those of charmed hadrons manifesting a basic structure that includes the fourth, charmed quark.

9 SUMMARY AND CONCLUSIONS

In somewhat less than two years of intense experimental activity, at least 13 new unstable hadrons have been discovered. They fall into two separate but related classes. One, the psion family, includes, first, the new vector mesons $\psi(3095)$, $\psi(3684)$, and $\psi(4414)$; second, the intermediate states $\chi(3415)$, $\chi(3500)$, and $\chi(3550)$; and third, the less well-established $\chi(3455)$ and $X(2800)$. The more recent assembly of new states includes the neutral and charged D mesons, D^0 (and presumably $\bar{D}^0$) at 1865 MeV/c^2 and D^+, D^- at 1876 MeV/c^2, together with the first new baryons, Λ_c at 2260 MeV/c^2 and Σ_c at 2450 MeV/c^2. All the characteristics of these new particles, their quantum numbers, the pattern of masses, and the variety of decay modes and widths, are in close correspondence with those of states that occur in a four-quark model of hadronic substructure.

The body of experimental evidence presented in this review strongly supports the notion that this small number of fundamental objects is responsible for the structure and interactions of the hadrons; however, there are gaps and quantitative discrepancies. Charmonium spectroscopy is still in a relatively primitive state; the pseudoscalar $^1S_0$ states have only a tenuous connection with reality; properties of the intermediate states are not sufficiently well-determined to permit definitive identification as ^3P levels; radiative transition rates are poorly known and not in good agreement with theoretical values; the structure of the higher radially excited ^3S states is very confused and their decay rates, particularly to states with charmed mesons, are essentially unknown. Only a small fraction of the charmed hadrons required by the model has yet been discovered. One may, in fact, also still feel uneasy about the value of R for e^+e^- annihilations at energies above the charmed-quark threshold.

The new discoveries have provided some basis for optimism that a correct basic theoretical framework has been invented. It remains to be seen, and no doubt will be seen in experiments in the near future, whether that structure is complete, or, at least, needs expansion to include still more, heavier quarks.

ACKNOWLEDGMENT

Much of what I know of the subject of this review has been learned from my colleagues, past and present, in the SLAC-LBL collaboration. They are: G. S. Abrams, M. S. Alam, J.-E. Augustin, A. M. Boyarski, M. Breidenbach, D. D. Briggs, F. Bulos, W. C. Carithers, S. Cooper, J. T. Dakin, R. G. DeVoe, J. M. Dorfan, G. E. Fischer, C. E. Friedberg, D. Fryberger, G. Goldhaber, D. Hitlin, G. Hanson, R. J. Hollebeek, B. Jean-Marie, J. Jaros, A. D. Johnson, J. A. Kadyk, R. R. Larsen, A. M. Litke, D. Lüke, B. A. Lulu, V. Lüth, H. L. Lynch, D. Lyon, R. J. Madaras, C. C. Morehouse, H. K. Nguyen, J. M. Paterson, M. L. Perl, F. M. Pierre, I. Peruzzi, M. Piccolo, T. Pun, P. Rapidis, B. Richter, B. Sadoulet, R. Schindler, R. F. Schwitters, J. Siegrist, W. M. Tanenbaum, G. H. Trilling, F. Vannucci, J. S. Whitaker, F. C. Winkelmann, J. Weiss, J. E. Wiss, and J. E. Zipse. I am greatly indebted to them for their efforts.

Particular thanks go to S. Cooper, M. Mandelkern, S. Shannon, M. Suzuki, and J. E. Wiss for corrections and clarifications that resulted from their careful reading of the text.

I am grateful for the hospitality and support of the Conselho Nacional de Pesquisas and the Universidade do Brasilia, Brazil where part of this review was prepared while I was a visiting professor in the Department of Physics.

Literature Cited

1. Particle Data Group, Trippe, T. G. et al 1976. Review of particle properties. *Rev. Mod. Phys.* 48: S1
2. Bjorken, J. D., Glashow, S. L. 1965. *Phys. Lett.* 11: 225
3. Glashow, S. L., Iliopoulos, J., Maiani, L. 1970. *Phys. Rev. D* 2: 1285
4. Carlson, C. E., Freund, P. G. O. 1972. *Phys. Lett. B* 39: 349
5. Appelquist, T., Politzer, H. D. 1975. *Phys. Rev. Lett.* 34: 43
6. Schwitters, R. F., Strauch, K. 1976. The physics of e^+e^- collisions. *Ann. Rev. Nucl. Sci.* 26: 89
7. Cosme, G. et al 1974. *Phys. Lett. B* 48: 159
8. Sakurai, J. J. 1969. *Currents and Mesons.* Chicago: Univ. Chicago Press
9. Nambu, Y., Sakurai, J. J. 1962. *Phys. Rev. Lett.* 8: 79
10. High-Energy Reactions Analysis Group, Bracci, E. et al 1972. Compilation of cross sections $I-\pi^-$ and π^+ induced reactions. *CERN/HERA 72-1*, CERN, Geneva, Switzerland
11. Whitmore, J. 1976. *Phys. Rep. C* 27: 188
12. Blobel, V. et al 1975. *Phys. Lett. B* 59: 88
13. Anderson, K. J. et al 1976. *Phys. Rev. Lett.* 37: 799
14. Silverman, A. 1975. *Proc. 1975 Int. Symp. Lepton Photon Interactions High Energies*, Stanford, Calif., p. 355
15. Ross, M., Stodolsky, L. 1966. *Phys. Rev.* 149: 1172
16. Anderson, R. et al 1970. *Phys. Rev. D* 1: 27
17. Behrend, H. J. et al 1975. *Phys. Lett. B* 56: 408
18. Okubo, S. 1963. *Phys. Lett.* 5: 165
19. Zweig, G. 1964. *CERN TH401, CERN TH412*, CERN, Geneva, Switzerland
20. Iizuka, J. 1966. *Suppl. Prog. Theor. Phys.* 37–38: 21
21. Rosenzweig, C. 1976. *Phys. Rev. D* 13: 3080
22. Appelquist, T., Politzer, H. D. 1975. *Phys. Rev. D* 12: 1404
23. Aubert, J. J. et al 1974. *Phys. Rev. Lett.* 33: 1404
24. Augustin, J.-E. et al 1974. *Phys. Rev. Lett.* 33: 1406
25. Abrams, G. S. et al 1974. *Phys. Rev. Lett.* 33: 1453
26. Bacci, C. et al 1974. *Phys. Rev. Lett.* 33: 1408
27. Criegee, L. et al 1975. *Phys. Lett. B* 53: 489
28. Becker, U. 1975. *New Directions in Hadron Spectroscopy, Proc. Summer*

Symp. Argonne Natl. Lab., July 7–10, 1975. Argonne, Ill., p. 209
29. Ting, S. C. C. 1975. See Ref. 14, p. 155
30. Aubert, J. J. et al 1975. *Nucl. Phys. B* 89:1
31. Knapp, B. et al 1975. *Phys. Rev. Lett.* 34:1044
32. Binkley, M. et al 1976. *Phys. Rev. Lett.* 37:571
33. Binkley, M. et al 1976. *Phys. Rev. Lett.* 37:574
34. Anderson, K. J. et al 1976. *Phys. Rev. Lett.* 36:237
35. Anderson, K. J. et al 1976. *Phys. Rev. Lett.* 37:799
36. Blanar, G. J. et al 1975. *Phys. Rev. Lett.* 35:346
37. Antipov, Y. M. et al 1976. *Phys. Lett. B* 60:309
38. Hom, D. C. et al 1976. *Phys. Rev. Lett.* 36:1236
39. Snyder, H. D. et al 1976. *Phys. Rev. Lett.* 36:1415
40. Hom, D. C. et al 1976. *Phys. Rev. Lett.* 37:1374
41. Büsser, F. W. et al 1975. *Phys. Lett. B* 56:482
42. Nagy, E. et al 1975. *Phys. Lett. B* 60:96
43. Boyarski, A. M. et al. 1975. *Phys. Rev. Lett.* 34:1357
44. Knapp, B. et al 1975. *Phys. Rev. Lett.* 34:1040
45. Camerini, U. et al 1975. *Phys. Rev. Lett.* 35:483
46. Gittelman, B. et al 1975. *Phys. Rev. Lett.* 35:1616
47. Nash, T. et al 1976. *Phys. Rev. Lett.* 36:1233
48. Ritson, D. M. 1976. *Particle Searches and Discoveries—1976, Vanderbilt. AIP Conf. Proc. No. 30, Part. Fields Subser. No. 11*, p. 75
49. Augustin, J.-E. et al 1975. *Phys. Rev. Lett.* 34:233
50. Wiik, B. H. 1975. See Ref. 14, p. 69
51. Lüth, V. et al 1975. *Phys. Rev. Lett.* 35:1124
52. Augustin, J.-E. et al 1975. *Phys. Rev. Lett.* 34:764
53. Jackson, J. D., Scharre, D. L. 1975. *Nucl. Instrum. Methods* 128:13
54. Braunschweig, W. et al 1976. *Phys. Lett B* 63:487
55. Jean-Marie, B. et al 1976. *Phys. Rev. Lett.* 36:291
56. Abrams, G. S. 1975. See Ref. 14, p. 25
57. Vannucci, F. et al 1977. *Phys. Rev. D* 15:1814
58. Gilman, F. J. 1975. *High Energy Physics and Nuclear Structure, Los Alamos, 9–13 June 1975. AIP Conf. Proc. No. 26,* p. 331
59. Gupta, V., Kögerler, R. 1975. *Phys. Lett. B* 56:473
60. Abrams, G. S. et al 1975. *Phys. Rev. Lett.* 34:1181
61. Tanenbaum, W. et al 1976. *Phys. Rev. Lett.* 36:402
62. Hilger, E. et al 1975. *Phys. Rev. Lett.* 35:625
63. Tanenbaum, W. et al 1975. *Phys. Rev. Lett.* 35:1323
64. Braunschweig, W. et al 1975. *Phys. Lett. B* 57:407
65. Whitaker, J. S. et al 1976. *Phys. Rev. Lett.* 37:1596
66. Feldman, G. et al 1975. *Phys. Rev. Lett.* 35:821
67. Trilling, G. H. 1976. Lawrence Berkeley Lab. Rep. LBL-5535
68. Biddick, C. J. et al 1977. *Phys. Rev. Lett.* 38:1324
69. Hughes, E. B. et al 1976. *Phys. Rev. Lett.* 36:76
70. Brown, L. S., Cahn, R. N. 1976. *Phys. Rev. D* 13:1195
71. Karl, G. et al 1976. *Phys. Rev. D* 13:1203
72. Kabir, P. K., Hey, A. J. G. 1976. *Phys. Rev. D* 13:3161
73. Heintze, J. 1975. See Ref. 14, p. 97
74. Bartel, W. et al 1976. *DESY 76/65*, DESY, Hamburg, Germany
75. Boyarski, A. M. et al 1975. *Phys. Rev. Lett.* 34:762
76. Schwitters, R. F. 1975. See Ref. 14, p. 5
77. Esposito, B. et al 1975. *Phys. Lett. B* 58:478
78. Bacci, C. et al 1975. *Phys. Lett. B* 58:481
79. Bacci, C. et al 1976. *Phys. Lett. B* 64:356
80. Barbiellini, G. et al 1976. *Phys. Lett. B* 64:359
81. Esposito, B. et al 1976. *Phys. Lett. B* 64:362
82. Tarjanne, P., Teplitz, V. L. 1963. *Phys. Rev. Lett.* 11:447
83. Amati, D. et al 1964. *Phys. Lett.* 11:190
84. Hara, Y. 1964. *Phys. Rev. B* 134:701
85. Maki, Z. et al 1964. *Prog. Theor. Phys. Kyoto* 32:144
86. Greenberg, O. W. 1964. *Phys. Rev. Lett.* 13:598
87. Han, M. Y., Nambu, Y. 1965. *Phys. Rev. B* 139:1006
88. Bars, I., Peccei, R. D. 1975. *Phys. Rev. D* 12:823
89. Feldman, G., Matthews, P. T. 1976. *Nuovo Cimento A* 31:447
90. Gaillard, M. K., Lee, B. W., Rosner, J. L. 1975. *Rev. Mod. Phys.* 47:277

91. De Rujula, A., Georgi, H., Glashow, S. L. 1975. *Phys. Rev. D* 12:147
92. Chanowitz, M., Gilman, F. J. 1976. *Phys. Lett. B* 63:178
93. Bethe, H. A., Salpeter, E. 1957. *Quantum Mechanics of One and Two Electron Atoms*. Berlin: Springer
94. Eichten, E. et al 1975. *Phys. Rev. Lett.* 34:369
95. Pumplin, J. et al 1975. *Phys. Rev. Lett.* 35:1538
96. Schnitzer, H. J. 1975. *Phys. Rev. Lett.* 35:1540
97. Harrington, B. J. et al 1975. *Phys. Rev. Lett.* 34:168
98. Eichten, E. et al 1976. *Phys. Rev. Lett.* 36:500
99. Barbieri, R. et al 1976. *Phys. Lett. B* 60:183
100. Barbieri, R. et al 1976. *Phys. Lett. B* 61:465
101. Siegrist, J. et al 1976. *Phys. Rev. Lett.* 36:700
102. Cester, R. et al 1976. *Phys. Rev. Lett.* 37:1178
103. Boyarski, A. M. et al 1975. *Phys. Rev. Lett.* 35:196
104. Goldhaber, G. et al 1976. *Phys. Rev. Lett.* 37:255
105. Peruzzi, I. et al 1976. *Phys. Rev. Lett.* 37:569
106. Knapp, B. et al 1976. *Phys. Rev. Lett.* 37:882
107. Wiss, J. et al 1976. *Phys. Rev. Lett.* 37:1531
108. Cazzoli, E. G. et al 1975. *Phys. Rev. Lett.* 34:1125
109. Benvenuti, A. et al 1975. *Phys. Rev. Lett.* 34:419
110. Barish, B. C. et al 1976. *Phys. Rev. Lett.* 36:939
111. Von Krogh, J. et al 1976. *Phys. Rev. Lett.* 36:710
112. Blietschau, J. et al 1976. *Phys. Lett. B* 60:207
113. Braunschweig, W. et al 1976. *Phys. Lett. B* 63:471
114. Burmester, J. et al 1976. *Phys. Lett. B* 64:369

TECHNICAL INFORMATION DEPARTMENT
LAWRENCE BERKELEY LABORATORY
UNIVERSITY OF CALIFORNIA
BERKELEY, CALIFORNIA 94720